


 Cite this: *RSC Adv.*, 2026, 16, 10193

# Multiscale modeling of graphene and carbon nanostructures: advances in atomistic, coarse-grained, and machine learning approaches

 Iman Najafipour<sup>\*a</sup> and Santanu Chaudhuri<sup>ab</sup>

Graphene, its derivatives such as graphene oxide and reduced graphene oxide, and related carbon nanostructures including carbon nanotubes, possess exceptional mechanical, thermal, and electronic properties. These features make them highly attractive for applications ranging from energy storage and filtration to flexible electronics and biomedical systems. Molecular simulation methods, including atomistic molecular dynamics, coarse grained modeling, and dissipative particle dynamics, have become essential tools for investigating the behavior of these materials at multiple length and time scales. This review presents recent advances in the modeling of graphene-based systems, highlighting how different simulation techniques are employed to explore mechanical deformation, defect evolution, thermal transport, and interfacial behavior. Special attention is given to the development of coarse-grained models, the role of force field selection, and the integration of machine learning to improve computational efficiency and predictive accuracy. Future directions include the use of high-performance computing, artificial intelligence assisted simulations, and scalable frameworks for large scale modeling. Overall, molecular simulations continue to play a critical role in the rational design and optimization of graphene-derived materials for advanced technological applications.

Received 5th December 2025

Accepted 1st February 2026

DOI: 10.1039/d5ra09422d

[rsc.li/rsc-advances](http://rsc.li/rsc-advances)

## 1. Introduction

Graphene, a single atomic layer of carbon atoms arranged in a hexagonal lattice through strong  $sp^2$  bonding, has attracted extensive scientific and industrial interest in recent years due to its extraordinary physicochemical properties.<sup>1–4</sup> The electronic structure of graphene is fundamentally determined by its two-dimensional hexagonal lattice, giving rise to linear energy dispersion near the K and K' points of the Brillouin zone. As a result, charge carriers in graphene behave as massless Dirac fermions, enabling ballistic transport and unconventional quantum phenomena.<sup>5</sup> The lightweight nature of carbon, combined with its anisotropic bonding, results in characteristics that often surpass those of traditional carbon and silicon-based materials.<sup>6</sup> These include a nonlinear mechanical response under strain,<sup>7</sup> superconductivity under specific configurations,<sup>8</sup> ballistic electron transport at room temperature,<sup>9</sup> and magnetism arising from edge states and topological defects.<sup>10</sup> Such properties position graphene as a highly versatile material, especially for next generation nanoelectronic applications demanding high performance, miniaturization, and energy efficiency.<sup>10</sup>

Beyond its remarkable electronic and mechanical characteristics, graphene also exhibits exceptional thermophysical properties that make it a benchmark material for nanoscale transport studies. At room temperature, its specific heat capacity is approximately  $700 \text{ J kg}^{-1} \text{ K}^{-1}$ , while its thermal conductivity ranges between  $2000$  and  $3500 \text{ W m}^{-1} \text{ K}^{-1}$ , depending on structural quality and measurement conditions.<sup>11–13</sup> Graphene's density ( $\sim 2.2 \text{ g cm}^{-3}$ ), negative thermal expansion coefficient ( $\sim -8 \times 10^{-6} \text{ K}^{-1}$ ), and extremely high Debye temperature ( $2100$ – $2300 \text{ K}$ ) further underline its unique phonon dynamics.<sup>14,15</sup> In addition, the Young's modulus ( $\sim 1 \text{ TPa}$ ), intrinsic tensile strength ( $\sim 130 \text{ GPa}$ ), and extraordinary electron mobility ( $\sim 2 \times 10^5 \text{ cm}^2 \text{ V}^{-1} \text{ s}^{-1}$ ) make graphene not only the strongest known material but also one of the most efficient for heat and mass transport at the atomic scale.<sup>11–13</sup>

The historical development of graphene research holds particular significance, as it illustrates how this material has evolved from the earliest stages of synthesis to the isolation of single layers, leading to a deeper understanding of its properties and the development of innovative applications. As shown in Table 1, the experimental journey of graphene spans over a century and encompasses key milestones, including the synthesis of graphite oxide, growth on substrates, and the isolation of single layers. This journey began in 1859, when Brodie independently synthesized graphite oxide.<sup>14</sup> This achievement laid the foundation for the chemical understanding of thin carbon layers and their functionalization,

<sup>a</sup>Department of Chemical Engineering, University of Illinois Chicago, Chicago 60607, IL, USA. E-mail: [inaja@uic.edu](mailto:inaja@uic.edu); [santc@uic.edu](mailto:santc@uic.edu)

<sup>b</sup>Department of Civil, Materials, and Environmental Engineering, University of Illinois Chicago, Chicago 60607, IL, USA



providing early insights into the feasibility of controlled exfoliation of graphite. In 1958, Hummers introduced his well-known method for graphite oxide synthesis, which represented a significant advancement in reproducibility and scalability, enabling the production of high-quality starting materials for systematic studies.<sup>15</sup> In the 1970s, the synthesis of monolayer graphene on silicon carbide (SiC) substrates allowed researchers to explore the intrinsic electronic and mechanical properties of graphene, although the method remained limited in terms of scalability.<sup>16</sup> This stage marked a critical step in understanding graphene's behavior and uncovering its unique characteristics, attracting significant attention from the scientific community for potential applications in electronics and advanced materials.

The true breakthrough occurred in 2004, when Novoselov *et al.* successfully isolated monolayer graphene using the simple and innovative "Scotch Tape" method.<sup>17</sup> This approach not only made graphene more accessible but also triggered a wave of fundamental and applied research worldwide, paving the way for the rapid development of this remarkable material. Subsequent studies revealed that graphene possesses a unique combination of exceptional mechanical strength, outstanding electrical and thermal conductivity, and optical transparency, making it an ideal material for electronics, energy storage, and flexible and printable technologies. By 2013, the importance of graphene had reached such a level that the number of publications in the field exceeded 40 papers per day, reflecting the widespread interest and focus of the scientific community on this material and its applications.<sup>18,19</sup>

This historical trajectory, as also highlighted in Table 1, emphasizes that graphene is not only a unique and extraordinary material but also a symbol of transformation in two-dimensional materials science, representing a convergence point between experimental and theoretical research. By integrating experimental advances with theoretical studies and sophisticated simulations, graphene has now become a central platform for the development of cutting-edge technologies, including nanoelectronics, energy storage, multifunctional materials, and flexible/printable devices, setting the stage for future research directions in the field.

As experimental exploration reached its practical limits, computational modeling emerged as an indispensable complement, allowing deeper insight into the atomic-level mechanisms governing graphene behavior. Building on the

remarkable capabilities of pristine graphene, research has expanded to include its functionalized derivatives such as graphene oxide (GO) and reduced graphene oxide (rGO).<sup>20</sup> These materials exhibit enhanced mechanical robustness, chemical versatility, and thermal stability,<sup>21</sup> enabling their use in sensors,<sup>22</sup> energy storage devices,<sup>23,24</sup> water purification membranes,<sup>25,26</sup> flexible electronics,<sup>27</sup> and various biomedical and drug delivery platforms.<sup>28,29</sup> The presence of oxygen-containing groups in GO and the partial restoration of the  $\pi$ -conjugated network in rGO offer tunable surface chemistry and modifiable interfacial behavior, enhancing their utility in application specific designs.<sup>30</sup>

As the complexity of graphene-based systems continues to grow, experimental approaches alone often fall short in characterizing phenomena that occur across atomic, molecular, and mesoscopic scales. Molecular simulation techniques have emerged as indispensable tools for exploring and predicting the behavior of graphene and its derivatives across multiple scales.<sup>31</sup>

The development of computational methods for graphene has progressed through several transformative stages. Between 1988 and 2000, the application of the Tersoff potential enabled the first atomistic studies of graphene lattice stability and basic mechanical properties.<sup>32</sup> This approach allowed researchers to understand bond lengths, angles, and elastic behavior at the atomic scale, although it was limited to small system sizes and could not capture reactive or defect-related phenomena. This period represents the earliest phase of graphene simulation, marking the first successful use of empirical potentials to describe the lattice and establish baseline mechanical behavior.

In 2001, the introduction of ReaxFF revolutionized the modeling of graphene by enabling reactive molecular dynamics simulations.<sup>33</sup> With ReaxFF, simulations could now account for bond breaking and formation, allowing the study of defects, oxidation processes, and chemical functionalization such as the formation of GO. This marked a significant step toward bridging the gap between static atomistic models and the dynamic, chemically active behavior observed experimentally. The shift from Tersoff to ReaxFF expanded simulation capability beyond structural stability to chemically evolving systems, representing the second major milestone in graphene modeling.

By 2011, dissipative particle dynamics (DPD) and coarse-grained (CG) models were implemented for graphene systems.<sup>34</sup> These approaches enabled researchers to study mesoscale phenomena, including self-assembly, defect

**Table 1** Illustrates the timeline of major scientific and technological milestones that shaped the development of graphene

Year	1859	1958	1975	2004	2010	2013
Event	Brodie independently synthesized graphite oxide	Graphite oxide independently synthesized by Hummers (Hummers' method)	Synthesis of monolayer graphene using silicon carbide substrates was achieved	Graphene was first isolated and characterized by Geim and Novoselov using the simple 'Scotch Tape' method. This work kick-started modern graphene research	The Nobel Prize in Physics was awarded to Geim and Novoselov for their pioneering work on two-dimensional atomic crystals	Academic publications reporting the use of graphene reached over 40 publications per day



clustering, and large-scale mechanical deformation. While atomic detail was sacrificed for efficiency, CG and DPD allowed simulations of systems orders of magnitude larger than those accessible by classical molecular dynamics, making it possible to investigate interactions with polymers, solvents, and other macromolecular components. This third stage in simulation development linked atomistic and mesoscale regimes, enabling multi-micron architectures and polymer-graphene composite behavior to be explored computationally.

In 2018, the integration of machine learning (ML) potentials into graphene simulations further expanded modeling capabilities.<sup>35</sup> ML potentials combine accuracy comparable to DFT with the computational efficiency needed for large-scale simulations, allowing researchers to explore complex chemical spaces and predict material behavior beyond the original training data. These methods facilitate rapid screening of functionalized and defective graphene structures, optimization of synthesis conditions, and multi-scale integration with CG and DPD models. This fourth milestone introduced data-driven simulation approaches capable of capturing both quantum-level accuracy and macroscale system sizes.

Together, these milestones mark the evolution of computational tools from empirical atomistic descriptions to data-driven predictive modeling, bridging multiple scales of material behavior. Collectively, these simulation advancements provide a multi-scale toolkit for studying graphene, from atomic-scale mechanical and electronic properties to mesoscale assembly and transport phenomena. They also allow predictive exploration of extreme conditions and novel material designs that are difficult or impossible to achieve experimentally. The historical progression of graphene simulation can now be understood as four major eras: (1) early Tersoff-based atomistic modeling (1988–2000), (2) the emergence of reactive simulations through ReaxFF (2001), (3) the rise of mesoscale CG/DPD methods (2011), and (4) adoption of machine learning potentials for DFT-level large-scale prediction (2018).

Approaches such as molecular dynamics (MD),<sup>36</sup> dissipative particle dynamics (DPD),<sup>37</sup> and coarse-grained (CG) modeling<sup>38–40</sup> have been employed to investigate a range of properties, including mechanical response, thermal conductivity, mass transport, interfacial interactions, and defect evolution. These techniques also facilitate the study of complex dynamic processes, such as surfactant adsorption and self-assembly, which are critical for optimizing material performance in real world applications.

In recent years, simulation techniques have not only complemented experimental approaches but also enabled predictive modeling of graphene systems under extreme conditions or at scales inaccessible to laboratory methods. The integration of machine learning into simulation workflows,<sup>41</sup> along with the development of hybrid multiscale frameworks,<sup>42</sup> has significantly expanded the scope and efficiency of computational materials science. These advances allow researchers to tailor properties such as mechanical strength, thermal transport, and electrokinetic behavior for targeted applications, while also uncovering structure property relationships that drive the rational design of novel materials.

This review provides a comprehensive overview of recent progress in the molecular simulation of graphene-based systems, with emphasis on simulation methodologies, key findings, and their implications for materials design. The sections that follow address mechanical behavior, thermal transport, self-assembly, electrokinetic phenomena, and the integration of machine learning into simulation workflows. Special attention is given to the advantages and limitations of each modeling approach, the importance of force field selection, and the need for experimental validation. The review concludes by outlining emerging research directions in high performance computing and data driven modeling aimed at bridging the gap between theoretical predictions and practical applications. The timeline of studies conducted on graphene, including experimental work, the development of its two-dimensional surface, and related simulation research, is schematically presented in Fig. 1. This figure summarizes the evolution of graphene from its initial discovery to recent advances.

## 2. Mechanical properties of graphene and carbon nanotubes

Graphene's exceptional mechanical strength and flexibility make it an ideal candidate for applications in flexible electronics, composites, and nanomechanical systems. Molecular simulations have played a central role in elucidating the fundamental deformation and failure mechanisms of graphene and its derivatives, providing insights that are difficult to obtain experimentally. Atomistic simulations have revealed the scale-dependent and defect-sensitive nature of graphene's mechanical behavior. Kim *et al.*<sup>43</sup> employed MD simulations to study the indentation response of monolayer and multilayer graphene using the reactive empirical bond order potential for in-plane interactions and the Lennard-Jones potential for interlayer forces.

Their results showed that the elastic modulus increased with the number of layers, stabilizing near 1 TPa beyond four layers, consistent with experimental data. Notably, fractures occurred at shallower indentation depths in multilayer systems, with the topmost layer failing first due to localized stress concentrations (Fig. 2).

Beyond in-plane stretching, graphene exhibits notable out-of-plane deformation behaviors such as wrinkling and buckling under mechanical loading. These responses are highly sensitive to boundary conditions, defect distribution, and the number of layers, influencing the stability and strength of suspended graphene membranes. Atomistic simulations have shown that out-of-plane ripples can act as stress relief mechanisms, delaying crack initiation and enabling reversible deformation under cyclic loading.<sup>43–45</sup> Chen *et al.* modeled the effect of grain size, strain rate, and temperature on polycrystalline graphene using structures generated by Voronoi tessellation.<sup>46</sup> Using the AIREBO potential, they demonstrated that decreasing grain size and increasing temperature led to lower fracture strength and Young's modulus, attributed to stress concentration and weakening at grain boundaries (Fig. 3). These findings underscore the need for careful microstructural control in applications involving dynamic loading or thermal cycling.



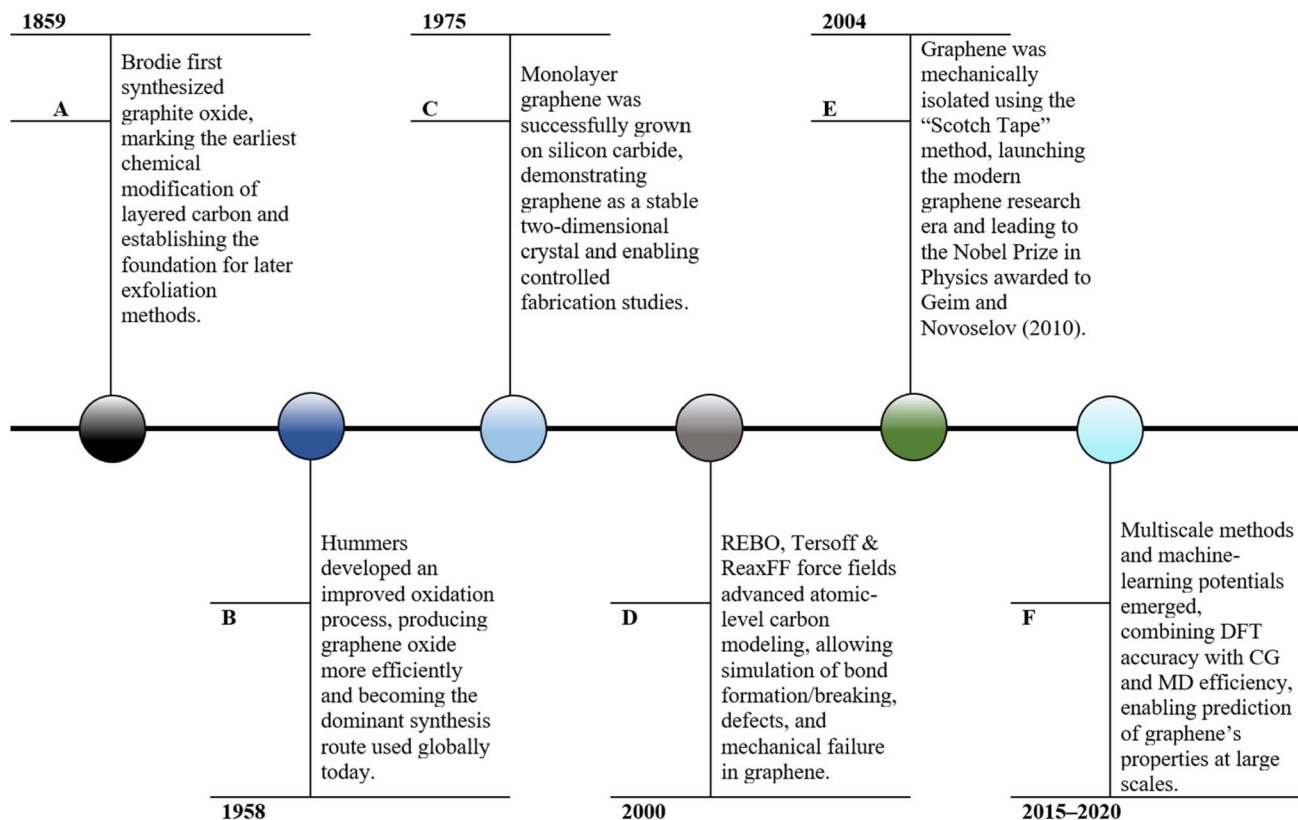


**Fig. 1** Timeline of graphene research highlighting key experimental, theoretical, and computational milestones: (A) early chemical oxidation of graphite (Brodie method), (B) development of the Hummers method for graphene oxide synthesis, (C) epitaxial growth of monolayer graphene on silicon carbide, (D) advances in atomistic modeling using REBO, Tersoff, and ReaxFF force fields, (E) isolation of monolayer graphene *via* the Scotch-tape method, and (F) emergence of multiscale and machine-learning-based modeling approaches bridging DFT, MD, and coarse-grained simulations.

Importantly, simulation predictions of Young's modulus and fracture strength align closely with experimental nano-indentation and tensile testing results, which report values

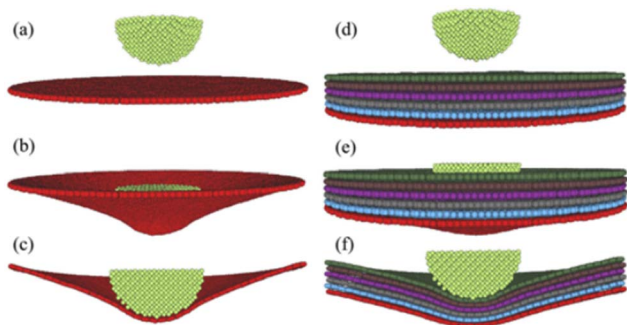


**Fig. 2** MD simulation of the indentation response in single-layer and six-layer graphene. Panels (a–c) depict the deformation sequence of a monolayer graphene sheet from its relaxed state to progressive indentation, while panels (d–f) illustrate the corresponding stages for a six-layer graphene model. Cross-sectional views of the indented structures are highlighted in (c) and (f).<sup>43</sup> Kim, H. J.; Seo, K. J.; Kim, D. E., Investigation of mechanical behavior of single- and multi-layer graphene by using molecular dynamics simulation, *International Journal of Precision Engineering and Manufacturing*, vol. 17, pp. 1693–1701, 2016. Reproduced with permission from Springer Nature, Copyright 2016.

ranging from 0.5 to 1 TPa for monolayer graphene depending on the presence of defects and substrate interaction. Such agreement validates the use of MD and CG approaches for predictive modeling and supports the development of simulation-guided material design strategies.<sup>7</sup>

The mechanical performance of graphene can also be tuned through chemical functionalization. Pei *et al.* conducted MD simulations to study hydrogenated graphene and found that partial hydrogenation (up to 30%) led to significant reductions in tensile strength and fracture strain, largely due to the conversion of  $sp^2$  bonds to weaker  $sp^3$  bonds.<sup>47</sup> At full hydrogenation (graphane), the material exhibited a 30% drop in Young's modulus and up to 65% loss in tensile strength compared to pristine graphene. These results suggest a tradeoff between chemical tunability and mechanical integrity Fig. 4.

Recent ReaxFF-based MD simulations by Li *et al.* explored hydrogen functionalized graphene allotropes and found that mechanical properties degrade markedly with increasing hydrogen coverage. At full hydrogenation, the Young's modulus can drop by  $\sim 70\%$  and tensile strength by  $\sim 90\%$ , primarily due to the conversion from  $sp^2$  to  $sp^3$  bonding and loss of structural integrity.<sup>48</sup> Lu *et al.* combined MD simulations and a thermodynamic continuum model to investigate how edge structure and passivation affect graphene nanoribbon mechanics.<sup>49</sup> Zigzag nanoribbons exhibited higher fracture strain and



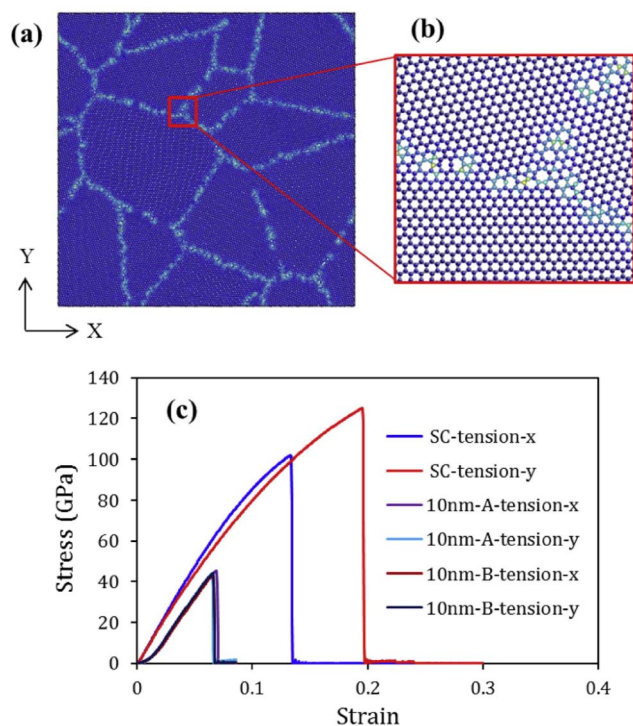


Fig. 3 MD simulation of polycrystalline graphene with an average grain size of 10 nm. (a) Model of a 30 nm  $\times$  30 nm graphene sheet with periodic boundary conditions applied along both  $x$  and  $y$  axes. (b) Enlarged view of a representative grain boundary. (c) Stress-strain responses of single-crystalline (SC) and polycrystalline graphene (10 nm grain size, samples A and B) under uniaxial tension in the  $x$  and  $y$  directions.<sup>46</sup> Reprinted from *Carbon*, vol. 85, M. Q. Chen, S. S. Quek, Z. D. Sha, C. H. Chiu, Q. X. Pei & Y. W. Zhang, "Effects of grain size, temperature and strain rate on the mechanical properties of polycrystalline graphene – a molecular dynamics study", pp. 135–146, Copyright 2015, with permission from Elsevier.

strength compared to armchair ones due to differences in crack nucleation behavior. Hydrogen passivation reduced edge energy, with a more pronounced impact on armchair configurations. This highlights the need for edge-specific engineering in nanoribbon-based devices. While atomistic simulations provide detailed insights, they are computationally expensive for large-scale systems. CG models have been developed to overcome this limitation. Ruiz *et al.* constructed a 4:1 CG model for multilayer graphene that retained hexagonal lattice symmetry and accurately captured directional mechanical responses under tension and shear (Fig. 5).<sup>38</sup>

Similarly, Liu *et al.* used a CG framework incorporating the Mie potential to replicate both in-plane and interlayer deformation at a fraction of the computational cost.<sup>39</sup> Their model reproduced key mechanical features such as compressive stress-strain behavior, bending stiffness, and self-folding dynamics (Fig. 6).

Complementing atomistic and polycrystalline studies, Jahanshahi *et al.* introduced a coarse-graining (CG) methodology to model the nonlinear mechanical behavior of FCC nanocrystals, demonstrating how Iterative Boltzmann Inversion (IBI) can derive effective interatomic potentials while

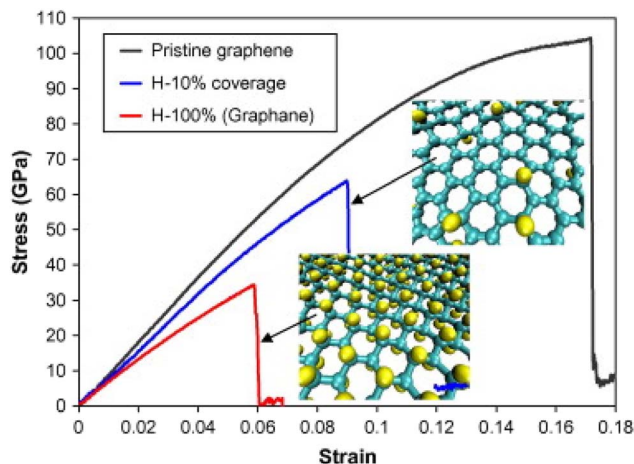


Fig. 4 Stress-strain behavior and structural configurations of hydrogen-functionalized graphene at 10% hydrogen coverage and fully hydrogenated graphene (graphane). Tensile loading is applied along the armchair direction. Hydrogen atoms are represented by yellow spheres.<sup>47</sup> Reprinted from *Carbon*, vol. 48, Q. X. Pei, Y. W. Zhang & V. B. Shenoy, "A molecular dynamics study of the mechanical properties of hydrogen functionalized graphene", pp. 898–904, Copyright 2010, with permission from Elsevier.

significantly reducing computational cost.<sup>50</sup> Their CG potential was validated against the Embedded Atom Method (EAM) potential, achieving comparable stress-strain predictions under

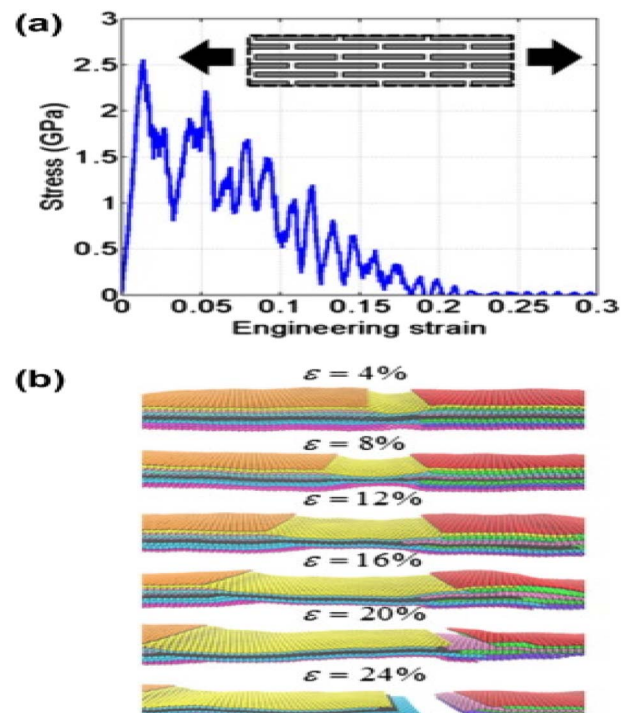
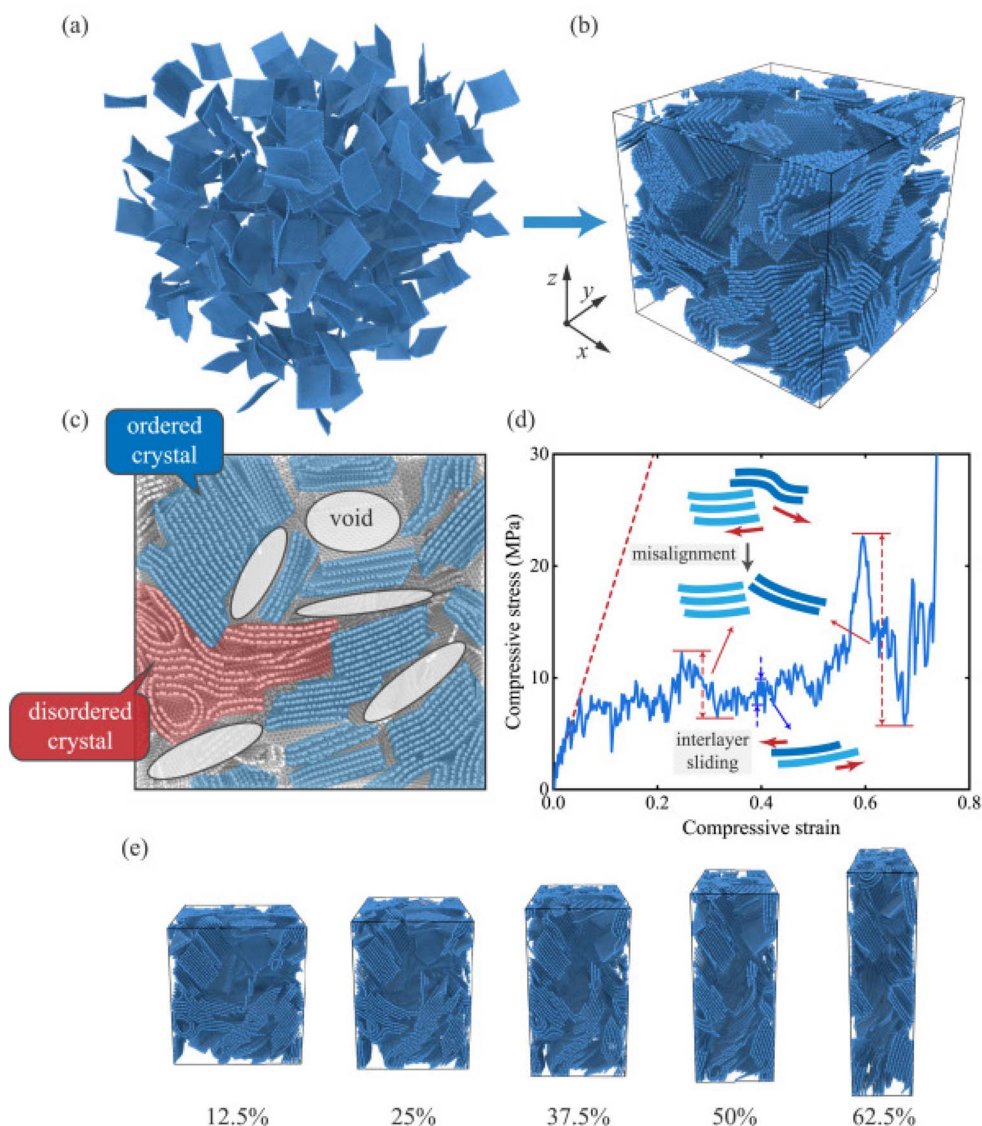


Fig. 5 Uniaxial tensile testing of a multilayer graphene (MLG) system. (a) Stress-strain curve with an inset showing the schematic architecture of the model (not drawn to scale). (b) Snapshots depicting the deformation sequence and failure process of the graphene layers.<sup>38</sup> Reprinted from *Carbon*, vol. 82, L. Ruiz, W. Xia, Z. Meng & S. Keten, "A coarse-grained model for the mechanical behavior of multi-layer graphene", pp. 103–115, Copyright 2015, with permission from Elsevier.





**Fig. 6** CG simulation of a large-scale graphene assembly. (a) Initial configuration composed of 320 square CG layers, each 200 Å wide, randomly distributed in the simulation box. (b) Final relaxed structure containing 267 520 CG with overall dimensions of 759 Å × 740 Å × 688 Å along x, y, and z directions. (c) Sectional view of the assembled structure. (d) Compressive stress–strain curve of the graphene assembly. (e) Snapshots illustrating deformation under varying compressive strains.<sup>39</sup> Reprinted from *Carbon*, vol. 178, Sihan Liu, Ke Duan, Li Li, Xuelin Wang, and Yujin Hu, "A multilayer coarse-grained molecular dynamics model for mechanical analysis of mesoscale graphene structures", pp. 528–539, Copyright 2021, with permission from Elsevier.

various loading conditions. Although initially developed for metals, this CG framework can be extended to graphene and other 2D materials to address the computational challenges of simulating large-scale systems. By adapting IBI-derived potentials for  $sp^2$  carbon networks, the mechanical response, deformation, and fracture of graphene nanoribbons and defect-engineered sheets could be captured efficiently, offering valuable insights for applications in nanocomposites, flexible electronics, and energy storage devices.

Bao *et al.* extended CG modeling to 3D graphene networks, simulating monolayer to six-layer assemblies under tension and compression.<sup>51</sup> The results showed that monolayer networks offered greater flexibility and interlayer slippage, while multilayer assemblies became more rigid (Fig. 7). The CG approach

effectively bridged atomistic detail and macroscopic behavior, enabling exploration of size and shape effects at larger scales.

Shear behavior and interlayer slippage are particularly critical in multilayer and stacked graphene systems. MD simulations by Shen & Wu have demonstrated that the interlayer shear modulus is orders of magnitude lower than the in-plane Young's modulus. This weak van der Waals coupling allows energy dissipation through interlayer sliding, which is especially important under bending or shear loads in multilayer paper-like composites.<sup>52</sup> Experimental measurements using pressurized bubble membranes report interlayer shear stress of ~40 kPa in bilayer graphene, far lower than interfacial strengths seen in layered composites, highlighting the pronounced size and registry dependence of multilayer shear.<sup>53</sup>



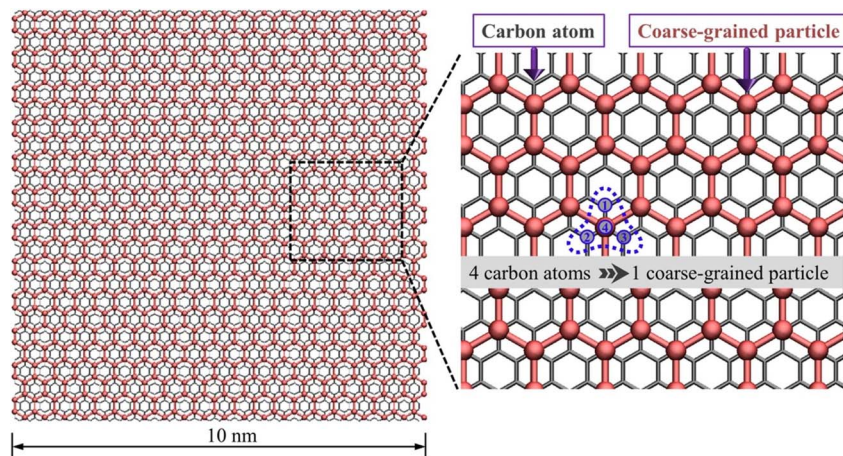


Fig. 7 Coarse-graining scheme for graphene, where four carbon atoms are represented by a single CG particle. The all-atom graphene structure is shown in gray, while the CG model is depicted in red.<sup>51</sup> Reprinted from *Applied Surface Science*, vol. 570, Qiang Bao, Zhenyu Yang, Zixing Lu & Xiaofan He, "Effects of graphene thickness and length distribution on the mechanical properties of graphene networks: a coarse-grained molecular dynamics simulation", Article 151023, Copyright 2021, with permission from Elsevier.

To simulate the mechanical behavior of carbon nanotubes (CNTs) at reduced computational cost, Liba *et al.* developed a DPD model of single-walled CNTs.<sup>54</sup> Their model preserved the tubular structure and elasticity of CNTs and successfully captured phenomena like bending, elongation, and tube-tube interactions. Notably, the simulation reproduced CNT zipping, a van der Waals-driven phenomenon observed during chemical vapor deposition (Fig. 8). While limited to single-walled CNTs and isotropic interactions, the model demonstrated the potential of DPD for mesoscale mechanical analysis of CNT-based systems.

Together, these atomistic and CG studies offer a multiscale understanding of how structure, functionalization, and dimensionality influence the mechanical behavior of graphene and carbon nanotubes. Such insights are critical for the design of nanostructured materials with tailored mechanical properties.

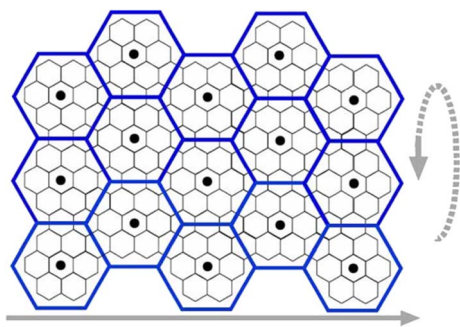


Fig. 8 Coarse-graining approach for a carbon nanotube (CNT), where 24 carbon atoms are grouped into a single CG particle. Solid dots indicate the lumped particles, while the solid arrow shows the tube axis and the dashed arrow represents the graphene wrapping process. The resulting model corresponds to an armchair CNT with a (6, 6) chirality.<sup>54</sup> Liba, O., Kaulzarić, D., Abrams, Z. R., Hanein, Y., Greiner, A. and Korvink, J. G., "A dissipative particle dynamics model of carbon nanotubes", *Molecular Simulation*, July 2008. Published by Taylor & Francis Ltd, Copyright 2008, reprinted by permission of the publisher (Taylor & Francis Ltd).

Molecular simulations have enabled detailed exploration of fracture processes in graphene under various loading conditions. Zhang *et al.* demonstrated that graphene's fracture toughness varies with crack length, lattice orientation, and edge termination, revealing a transition from brittle to quasi-ductile behavior at nanoscale dimensions.<sup>55</sup> Dewapriya and Meguid conducted MD simulations of out-of-plane crack propagation in graphene sheets, revealing that rippling significantly influences crack dynamics and enhances fracture resistance under certain loading orientations.<sup>56</sup>

Temperature and strain rate play critical roles in modulating graphene's mechanical response. Wei *et al.* used MD to show that pentagon-heptagon topological defects influence thermal softening and strain localization in graphene sheets, particularly under high temperatures.<sup>57</sup> MD simulations and continuum modeling have shown that thermal ripples in monolayer graphene lead to nonlinear stiffening and strain stiffening under compressive or biaxial loading conditions. Singh and Hennig demonstrated a temperature- and layer-dependent scaling of ripple amplitudes, while Mauri *et al.* explored the distinct thermal fluctuation behavior in bilayer graphene, highlighting the impact of interlayer coupling on flexural stability under zero tension.<sup>58,59</sup> These behaviors are crucial for thermal management and high-strain-rate applications.

The mechanical properties of CNTs are highly sensitive to their chirality and the presence of structural defects. Yakobson, Brabec, and Bernholc performed molecular dynamics simulations showing that carbon nanotubes undergo snap-through buckling and kinking under bending and compressive loads, with critical strain highly dependent on chirality and diameter.<sup>60</sup> Lu and Bhattacharya used atomistic simulations to show that Stone-Wales (SW) defects substantially reduce the tensile strength and stiffness of single-walled carbon nanotubes, with greater sensitivity in zigzag configurations and increased mechanical variability under strain.<sup>61</sup> These studies highlight the need to account for atomic topology in CNT mechanics.



Theoretical and experimental studies indicate that the Young's modulus of carbon nanotubes (CNTs) is at least as high as that of graphite and can be even higher for small single-walled CNTs (SWNTs). Our experiments show that the modulus of multi-walled CNTs (MWNTs) depends on the degree of order within the tube walls; as disorder increases, the modulus decreases, and the variability of measured values grows. These results highlight the importance of controlling CNT structure to achieve uniform mechanical properties in composites.<sup>62</sup> Graphene and CNTs are widely used as reinforcements in polymer nanocomposites, where interfacial load transfer governs mechanical performance. Arash, Park, and Rabczuk developed a CG model to simulate CNT pull-out and stress transfer in polymer nanocomposites. Their simulations demonstrated how CNT volume fraction, aspect ratio, and interfacial bonding affect the elastic modulus and failure strength of the composite system.<sup>63</sup> Chen *et al.* reviewed the interfacial characteristics of CNT-polymer composites, highlighting the roles of surface functionalization, dispersion quality, and matrix compatibility in determining pull-out behavior and load transfer efficiency.<sup>64</sup>

Graphene-reinforced polymer nanocomposites have garnered significant attention due to their tunable mechanical properties and processing-dependent morphologies. Lin *et al.* employed a multiscale simulation approach, combining DPD and finite element method (FEM), to evaluate the dispersion and mechanical performance of poly(methyl methacrylate) (PMMA) nanocomposites reinforced with pristine graphene (GN), functionalized graphene (FGN), and polymer-coated PMMA@FGN.<sup>65</sup> Their DPD simulations revealed that surface functionalization enhances exfoliation and alignment of graphene under shear flow, while pristine graphene tends to agglomerate. PMMA@FGN nanofillers provided optimal dispersion due to steric stabilization from polymer coatings. FEM analysis showed a corresponding increase in both tensile and shear moduli following the hierarchy PMMA@FGN > FGN > GN. These results underscore the importance of interface engineering and shear processing in optimizing the mechanical performance of graphene-based nanocomposites.<sup>65</sup> These simulation-derived trends indicate that experimentally optimizing graphene dispersion and interfacial bonding is critical for maximizing mechanical reinforcement in graphene-polymer composites.

Table 2 presents a comprehensive comparison of three fundamental mechanical properties: fracture strain, fracture strength, and Young's modulus obtained from four different methodologies: experimental,<sup>7</sup> molecular dynamics

(atomic),<sup>66–68</sup> machine learning (ML),<sup>69</sup> and coarse-grained (CG).<sup>38</sup> For fracture strain, the experimental value ( $25 \pm 2\%$ ) serves as the reference, indicating that the material can elongate significantly before failure. The ML model predicts  $23 \pm 2\%$ , showing excellent agreement and confirming its ability to replicate the ductile behavior observed in experiments. The atomic simulations yield a broader range (13–38%), which reflects the variability introduced by atomic-scale effects such as defects, strain rate, and boundary conditions. In contrast, the CG model gives smaller values (11–15%), suggesting an underestimation of ductility due to simplifications in its coarse-grained representation. For fracture strength, the experimental measurement ( $130 \pm 10$  GPa) represents the actual resistance of the material to breaking under stress. The ML prediction ( $125 \pm 5$  GPa) aligns very closely with this benchmark, confirming the model's strong predictive capability. The atomic simulations produce a wide range (90–195 GPa), consistent with their sensitivity to local atomic arrangements and simulation conditions, while the CG model (64–81 GPa) again underestimates the strength because it neglects fine atomic interactions that contribute to load-bearing capacity. In the case of Young's modulus, which reflects the material's stiffness, all four approaches show excellent consistency. The experimental value ( $1.0 \pm 0.1$  TPa) overlaps with ML ( $1.0 \pm 0.05$  TPa), MD (0.8–1.13 TPa), and CG (0.9–1.18 TPa) results. This agreement indicates that stiffness, as a largely elastic and structure-averaged property, is well captured even by simplified or data-driven models. Overall, Table 2 demonstrates that the machine learning approach reproduces experimental data with high precision, while molecular dynamics captures the realistic variability of material behavior, and coarse-grained simulations, despite being computationally efficient, tend to underestimate fracture-related properties, though they still provide reliable predictions for elastic stiffness.

Fig. 9 comparison of mechanical properties obtained from four different approaches (atomic, experimental, machine learning, and coarse-grained) is presented in a radar chart. This figure illustrates three fundamental mechanical properties along the radial axes: fracture strain, representing the material's ductility; fracture strength, indicating its resistance to breaking; and Young's modulus, reflecting its stiffness. As observed, Young's modulus remains nearly constant ( $\sim 1$  TPa) across all methods, demonstrating that each approach accurately predicts the stiffness of the material. In contrast, fracture strain and fracture strength vary more noticeably among methods: the experimental data (blue line) serve as the reference standard, the machine learning model (orange line) closely matches these

**Table 2** Comparison of fracture strain, fracture strength, and Young's modulus obtained from experimental, molecular dynamics (atomic), machine learning (ML), and coarse-grained (CG) approaches; ML closely matches experimental data, MD captures realistic variability, and CG tends to underestimate mechanical properties

Property	Unit	Experimental	Molecular dynamics (atomic)	Machine learning (ML)	Coarse-grained (CG)
Fracture strain	%	$25 \pm 2$	13–38	$23 \pm 2$	11–15
Fracture strength	GPa	$130 \pm 10$	90–195	$125 \pm 5$	64–81
Young's modulus	TPa	$1.0 \pm 0.1$	0.8–1.13	$1.0 \pm 0.05$	0.9–1.18



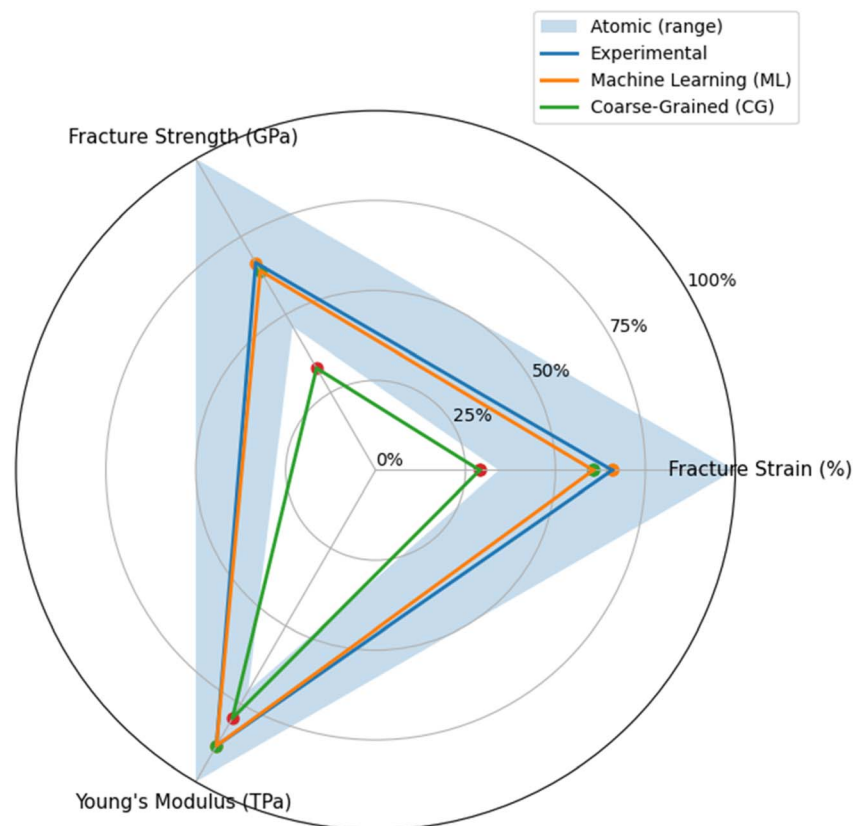


Fig. 9 Comparison of mechanical properties (Young's modulus, fracture strength, and fracture strain) obtained from four different approaches: atomic, experimental, machine learning (ML), and coarse-grained (CG). The ML model shows the closest agreement with experimental data, while the atomic model captures the realistic variability of the material, and the CG model tends to underestimate the mechanical properties.

experimental values, showing high predictive accuracy, the atomic simulations (light blue shaded area) capture a broad and realistic range of variability inherent to atomic-scale behavior, and the coarse-grained model (green line), while computationally simpler, tends to underestimate both strain and strength. Overall, the ML model offers the most accurate predictions, the atomic approach provides the most realistic variability, and the CG model, though faster and less detailed, offers an efficient yet conservative estimation of material failure behavior.

### 3. Thermal and mass transport in graphene-based systems

The exceptional thermal conductivity and selective mass transport properties of graphene and its derivatives are critical for applications in electronics, energy storage, desalination, and membrane technologies. Recent studies show that the synthesis and structure of graphene and its derivatives, such as CVD growth and large-scale production, enable uniform, stable films and nanomembranes with optimized thermal and mass transport performance.<sup>70</sup> Molecular simulations, particularly non-equilibrium molecular dynamics (NEMD), CG methods, and DPD, have been widely used to investigate the transport phenomena in these nanomaterials. This section reviews key advances in modeling thermal and mass transport in graphene

systems, focusing on interatomic potential selection, structural modifications, and multiscale modeling approaches.

Transport through graphene-based nanochannels depends strongly on the degree of confinement and on the appropriate hydrodynamic boundary condition. A simple geometric indicator is the confinement ratio  $H/d$ , where  $H$  is the effective channel height (or CNT diameter) and  $d$  is the characteristic molecular diameter (for water,  $d \sim 0.27\text{--}0.30$  nm). When  $\frac{H}{d}$  approaches only a few molecular diameters (*i.e.*, sub-1–2 nm confinement), molecular layering, discrete hydration structure, and even single-file-like motion can emerge, and continuum assumptions become increasingly unreliable. In addition, the Knudsen number  $\text{Kn} = \lambda/H$  is often used as a regime indicator in rarefied-gas flows; although liquid water is not a dilute gas, a similar conceptual distinction between continuum-like and molecularly dominated transport applies: when the confinement length scale becomes comparable to the relevant microscopic length scale, transport becomes increasingly non-continuum and sensitive to interfacial physics. For pressure-driven flow, the Péclet number  $\text{Pe} = UH/D$  (with mean velocity  $U$ , channel height  $H$ , and diffusivity  $D$ ) indicates whether advection or diffusion dominates mass transport. Importantly, nanoscale flows in CNTs and graphene channels are also highly sensitive to the assumed wall boundary condition: below  $\sim 1\text{--}2$  nm confinement, continuum assumptions and no-slip



boundaries become unreliable; slip length and interfacial friction can dominate predicted flux, so “enhancement factors” should be interpreted in light of boundary-condition sensitivity and validated slip models. This has been discussed in recent critical assessments and scale-effect treatments for CNT water transport and slip-modified descriptions, and supported by experimental demonstrations of large, radius-dependent slip-length in CNTs.<sup>71–73</sup>

Thermal conductivity ( $\kappa$ ) in graphene is among the highest of all known materials, but it is highly sensitive to structural factors and simulation settings. Thermal conductivity in graphene exhibits a wide range in experimental measurements, reported between 1500 and 5300 W m<sup>-1</sup> K<sup>-1</sup>, reflecting variations in sample quality, defects, and measurement conditions.<sup>12,74–76</sup>

Recent studies continue to refine our understanding of thermal transport in graphene-related systems. For example, Li and *et al.*, used molecular dynamics and machine-learning frameworks to elucidate thermal transport in defective graphene/graphyne van der Waals heterostructures, highlighting the interplay between structural defects and phonon transport in engineered 2D carbon networks.<sup>77</sup>

Molecular Dynamics (MD) simulations predict lower values, ranging from 350 to 3000 W m<sup>-1</sup> K<sup>-1</sup>, due to finite-size effects, limited sampling time, and incomplete representation of long-wavelength phonon transport.<sup>76,78–86</sup> In contrast, Machine Learning (ML) approaches estimate  $\kappa$  at approximately 3600 W m<sup>-1</sup> K<sup>-1</sup>, lying within the mid-range of experimental data.<sup>87</sup> These numerical ranges provide a useful reference for evaluating the predictive accuracy of simulations and guide the selection of interatomic potentials in subsequent NEMD studies. Si *et al.* systematically evaluated interatomic potentials for modeling thermal transport in graphene using NEMD simulations across a temperature range of 200–500 K (Fig. 10).<sup>88</sup> They found that the optimized Tersoff (opt-Tersoff) potential provides the best agreement with experimental data. It captures both the reduction in  $\kappa$  with increasing temperature and the role of interlayer phonon scattering.

To improve predictive accuracy in multilayer and hybrid systems, hybrid models combining opt-Tersoff with van der Waals potentials (*e.g.*, registry-dependent potentials) are often used. These models better capture out-of-plane phonon contributions. Zhang, Lee, and Cho examined thermal transport in graphene containing vacancy defects and showed that increasing vacancy concentration leads to significant reductions in thermal conductivity due to enhanced phonon scattering and reduced lifetimes of acoustic modes.<sup>89</sup> Similarly, Bouzerar *et al.* demonstrated that vacancies dramatically alter phonon lifetimes and limit lattice thermal conductivity in graphene sheets.<sup>90</sup> Jiang *et al.* reported that isotope doping in graphene nanoribbons reduces thermal conductivity due to phonon localization effects, with narrower ribbons experiencing more pronounced suppression. Their findings suggest that isotope engineering can be used to tailor phonon transport in low-dimensional systems.<sup>91</sup>

Thermal conductivity in rGO shows further complexity. Renteria *et al.* investigated the impact of thermal annealing on

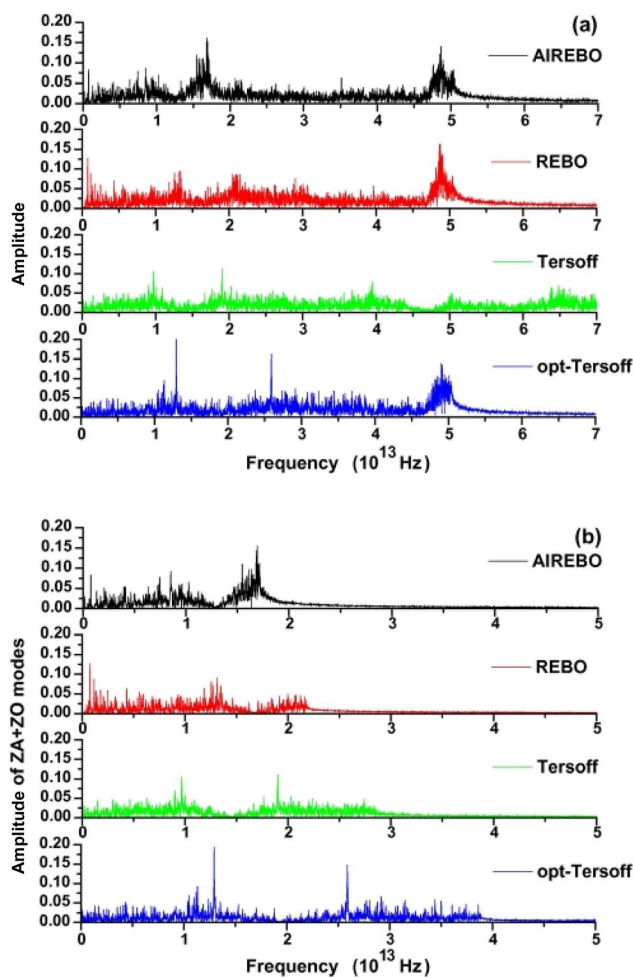


Fig. 10 Phonon spectrum analysis for different interatomic potential models at 300 K: (a) total vibrational power spectrum and (b) power spectra of the out-of-plane acoustic (ZA) and optical (ZO) phonon modes.<sup>88</sup> Reprinted from *International Journal of Heat and Mass Transfer*, vol. 107, Chao Si, Xiao-Dong Wang, Zhen Fan, Zhi-Hai Feng, “Impacts of potential models on calculating the thermal conductivity of graphene using non-equilibrium molecular dynamics simulations”, pp. 450–460. Copyright 2017, with permission from Elsevier.

the thermal conductivity of rGO films and found that in-plane conductivity increased significantly with oxygen removal, reaching values above 60 W m<sup>-1</sup> K<sup>-1</sup>, while cross-plane conductivity decreased to near-insulating levels.<sup>92</sup> Park *et al.* further demonstrated, through both experiments and simulations, that increasing rGO content in polymer composites enhances thermal conductivity due to improved heat percolation pathways.<sup>93</sup> These studies underscore the critical influence of defects, chemistry, and dimensionality on graphene's heat conduction behavior. Structural asymmetry enables directional heat transport, thermal rectification, in 2D materials. Yousefi *et al.* conducted NEMD simulations of nanoporous graphene (NPG), revealing a drastic reduction in thermal conductivity up to two orders of magnitude lower than pristine graphene due to enhanced phonon scattering at pore edges.<sup>94</sup> Their results showed direction-dependent heat transport, with the armchair



direction exhibiting higher  $\kappa$  than the zigzag direction, attributed to anisotropic phonon dispersion.

At the nanoscale, predicted mass flux through carbon nanotubes and graphene-based channels depends critically on the assumed hydrodynamic boundary condition at the solid-liquid interface. Classical continuum models with a no-slip boundary condition substantially underestimate experimentally observed flow rates in CNTs, whereas introducing a finite slip length can increase predicted permeability by several orders of magnitude. Karim *et al.*, critically showed that reported “flow enhancements” in CNT membranes are highly sensitive to the choice of slip boundary condition and that slip-modified Hagen–Poiseuille descriptions are required to reconcile simulations and experiments at small diameters. Molecular-scale analyses further demonstrate that interfacial friction is not constant but depends on nanotube curvature, with reduced friction and enhanced slippage emerging in narrow CNTs, as elucidated by Falk *et al.* Experimental measurements by Secchi *et al.*, directly validated this picture by quantifying large, radius-dependent slip lengths in individual CNTs, confirming that boundary-condition assumptions—and not only finite-size effects—play a dominant role in determining nanoscale flux. Consequently, transport predictions in sub-nanometer to few-nanometer channels must be interpreted in light of boundary-condition sensitivity and validated slip models rather than relying solely on no-slip continuum assumptions.<sup>71–73</sup>

Farzadian *et al.* extended this concept to graphene/BCN hybrid structures, showing that rectification can be enhanced by engineering the grain boundary orientation and applying mechanical strain.<sup>95</sup> Among three BCN configurations studied, BCN-1 with armchair-oriented interfaces achieved rectification ratios up to 68% under a temperature gradient of 100 K. These findings suggest the viability of graphene-based thermal diodes *via* nanoscale heterostructuring. Hu *et al.* performed MD simulations showing that asymmetric graphene nanoribbons exhibit notable thermal rectification due to edge chirality and geometric asymmetry. Their study established that narrower ribbons and asymmetric edge designs enhance rectification effects.<sup>96</sup> Zhang *et al.* further studied in-plane hexagonal BCnN/graphene heterojunctions and demonstrated that interfacial phonon mismatch in these systems can yield measurable rectification, especially when combining structural asymmetry with interfacial engineering.<sup>97</sup> Recent studies have shown that graphene/BCN hybrid structures offer tunable thermal transport properties due to the interplay of phonon spectra at the interface. Using NEMD simulations, a study on graphene/BCN hybrids investigated thermal rectification with respect to BCN configuration, grain boundary orientation, and mechanical strain.<sup>95</sup> Among various designs (BCN-1, BCN-2, BCN-3), the BCN-1 configuration exhibited the highest rectification ratio, reaching up to 68% under a 100 K temperature gradient for armchair-oriented boundaries, while zigzag interfaces showed negligible TR due to competing phonon scattering effects. The results further emphasized the role of Kapitza resistance at the graphene-BCN interface, driven by phonon density-of-states mismatch across the interface, leading to direction-dependent heat flow. Mechanical strains were found to modulate TR,

with moderate strains (<5%) enhancing phonon transport in BCN-1 and BCN-2, while BCN-3 showed diminished rectification at higher strains. Analysis of the phonon DOS revealed that interfacial phonon mismatch and strain engineering are critical design parameters for graphene-based thermal diodes and nanoscale heat management devices.<sup>95</sup>

Wu *et al.* investigated the thermal conductance of graphene/MoS<sub>2</sub> heterostructures *via* NEMD simulations and observed a conductance of approximately 8.95 MW m<sup>-2</sup> K<sup>-1</sup> at room temperature, which increased with thermal bias. They also found that introducing single-carbon vacancies at the interface could enhance conductance by nearly 90%, offering a viable route toward weak thermal rectification through defect engineering. These findings demonstrate that phonon band engineering and heterostructuring are powerful tools for controlling heat flow in nanodevices.<sup>98</sup> Mass transport through GO and rGO membranes is governed by pore structure, functionalization, and water-graphene interactions. Zeng *et al.* developed a CG DPD model to simulate heat and moisture diffusion in GO-PVP/PVDF composite membranes, addressing limitations of traditional macro- and atomistic-scale models.<sup>99</sup> Their approach incorporated Fast Fourier Transforms and CG beads to simulate mesoscale diffusion and surface wetting behavior.

Joshi *et al.* conducted experimental and theoretical investigations into GO membranes and demonstrated that molecular sieving is governed by interlayer spacing, which can be tuned by humidity and oxidation level. Their study showed that water molecules permeate rapidly while ions are rejected due to confinement and electrostatic interactions.<sup>100</sup> Mi further developed GO membranes for nanofiltration and desalination, highlighting their scalability and tunable selectivity through flake alignment and oxidation control.<sup>101</sup> They highlighted that membrane performance is tunable *via* humidity, oxidation level, and flake alignment. Yang *et al.* used MD simulations and experiments to investigate ion sieving in ultrathin GO membranes, showing that hydrated ions such as Na<sup>+</sup> and Cl<sup>-</sup> experience size-selective transport driven by dehydration barriers and channel confinement. Their results underline the importance of interlayer tuning and surface chemistry for selective permeability.<sup>102</sup>

Composite membranes have numerous applications, but accurately modeling and manipulating heat and mass transfer through these structures remains challenging. Previous attempts using either micro-scale all-atom MD simulations<sup>103</sup> or macro-scale resistance-in-series models<sup>104</sup> have significant limitations. Macro-scale resistance models, while computationally efficient, operate as black-box lumped-parameter approaches that fail to account for mesoscale structural features such as surface roughness, pore sizes, and molecular-level interactions. In contrast, all-atom MD simulations can provide detailed molecular-level insights into phenomena like pore hydration, solute diffusion, and interfacial dynamics, but they are computationally expensive and limited in their ability to model large or complex systems due to the high level of molecular detail required. The simulations revealed that porosity, surface energy, and filler distribution control water uptake and mass flux through the membrane. The model



successfully captured the trade-off between permeability and selectivity, providing a robust platform for optimizing GO-based filtration membranes for desalination, pervaporation, and humidity control applications. These findings suggest that, experimentally, precise control over channel size, surface functionalization, and ionic environment is essential for tuning permeability and selectivity in graphene-based membranes.

The dispersion stability of graphene and GO in aqueous environments significantly affects their performance in filtration, sensing, and printable electronics. CG and atomistic simulations have played a key role in elucidating the molecular mechanisms governing aggregation, interfacial interactions, and the impact of solvent composition. Williams and *et al.*, introduced CG models for pristine and functionalized graphene using a 4 : 1 mapping scheme and a Martini-compatible water model.<sup>105</sup> Their simulations showed that pristine graphene strongly aggregates due to van der Waals forces ( $\Delta F = -316 \text{ kJ mol}^{-1}$ ), while GO, owing to its surface functional groups, remained dispersed under neutral and basic pH due to electrostatic repulsion. The aggregation free energy for protonated GO ( $-109 \text{ kJ mol}^{-1}$ ) was significantly lower than for pristine graphene, supporting experimental trends. Entropic effects also played a critical role, with surface heterogeneity in GO hindering ordered stacking. These models can be adapted to simulate size-dependent dispersion, pH-triggered aggregation, and co-solvent effects in scalable membrane design. Table 3 demonstrates a regime guidance for modelling transport, electrokinetic, and dispersion in graphene-based systems.<sup>71–73</sup>

Limitations and regime boundaries of CG/DPD models: while coarse-grained (CG) and dissipative particle dynamics (DPD) models enable access to mesoscopic length and time scales, their applicability is limited in regimes where transport is governed by molecular discreteness. In sub-nanometer CNTs and narrow GO galleries, single-file-like constraints, strong hydrogen-bond cooperativity, and highly correlated (sometimes burst-like or ballistic) motion can emerge under confinement,

as demonstrated by atomistic simulations of water confined in carbon nanotubes. In this regime, CG representations cannot reproduce correlated molecular motion or discrete hydration structure; notably, previous studies reported a ballistic regime at short times, transitioning to Fickian diffusion at longer timescales in narrow CNTs. Similarly, hydration-shell distortion and ion dehydration penalties dominate ion selectivity in angstrom-scale channels, requiring atomistic resolution for quantitative predictions. In such regimes, CG/DPD models are most reliable for capturing mesoscale morphology, swelling, and dispersion trends after calibration to atomistic or experimental benchmarks. Importantly, thermodynamic consistency of CG models should be explicitly verified, including preservation of potentials of mean force, solvation free energies, and pressure tensors, particularly when free-energy differences govern aggregation or selectivity. This is illustrated by prior CG studies that report markedly different interaction free energies for pristine graphene *versus* graphene oxide, emphasizing the need for careful validation when extending CG models beyond their calibrated regime.<sup>106,107</sup>

Tang *et al.* used MD simulations to investigate how pH and electrolyte composition affect GO aggregation. They showed that divalent ions like  $\text{Ca}^{2+}$  strongly promote sheet-to-sheet restacking, while acidic pH neutralizes surface charges, increasing aggregation propensity. In contrast, basic pH and monovalent ions like  $\text{Na}^+$  favored dispersion through electrostatic stabilization.<sup>108</sup> Their free energy profiles confirmed that electrostatic interactions dominate aggregation thermodynamics in aqueous media. Wu and Yang explored surfactant-assisted dispersion using CG MD simulations of nonionic surfactants on graphene. Their study revealed that PEO chains can adsorb along sheet edges and stabilize graphene suspensions *via* steric hindrance, with the dispersion efficiency depending on chain length and concentration.<sup>109</sup> Shih *et al.* used MD simulations and experiments to explore how pH and temperature influence the colloidal stability of GO. Their study

**Table 3** Regime guidance for modeling transport, electrokinetic, and dispersion in graphene-based systems

Application	Key length scale	Recommended modeling level	Rationale
CNT water transport	CNT diameter 0.6–2 nm	Atomistic MD (validated slip/friction models)	Sub-nanometer confinement leads to chain-like ordering, strong hydrogen-bond cooperativity, and highly correlated (burst-like or ballistic) motion; continuum no-slip models underestimate flux
GO membranes (water/ions)	GO interlayer spacing 0.7–1.2 nm	Atomistic MD for selectivity; CG/DPD for mesoscale swelling	Hydration-shell distortion, ion dehydration penalties, and confinement-driven correlations dominate transport and selectivity at angstrom–nanometer scales
Electrokinetics in graphene channels	Debye length $\lambda_D$ vs. channel height $H$	Continuum valid if $\lambda_D/H \ll 0.1$ ; atomistic/CG otherwise	Strong EDL overlap, ion-wall interactions, and charge regulation invalidate mean-field electrokinetic assumptions
Graphene ink dispersion/assembly	>10 nm to $\mu\text{m}$ scale	CG/DPD	Collective hydrodynamics, aggregation, and solvent-mediated interactions dominate; atomistic details unnecessary after calibration



demonstrated that increased temperature weakens hydration shells around functional groups, promoting aggregation, while basic pH improves dispersion by enhancing surface charge repulsion.<sup>110</sup>

Simulations of thermal and mass transport in graphene materials provide critical insight into the structure–function relationships driving device performance. Accurate thermal modeling hinges on appropriate interatomic potentials, treatment of phonon scattering, and representation of dimensional effects. For mass transport, CG and DPD approaches offer valuable scalability while preserving essential chemical and interfacial features. Emerging directions include integrating machine learning to accelerate transport property predictions across diverse chemistries and morphologies. Coupled simulations of thermal and mass flux could enhance the design of multifunctional membranes and energy devices. Further efforts are also needed to link simulations *situ* experimental data, enabling validation and refinement of multiscale models under realistic conditions.

## 4. Simulation of interaction and assemblies

Molecular simulations have played a pivotal role in understanding the self-assembly, interfacial interactions, and dispersion behavior of graphene and related nanomaterials. These studies are essential for applications in composite processing, surfactant stabilization, drug delivery, and biosensing. This section is organized into thematic subsections that capture how CG, DPD, MD, and analytical models have been used to investigate assembly behavior in various chemical and environmental contexts.

### 4.1. Self-assembly of graphene in aqueous and surfactant environments

CG simulations offer an efficient way to capture large-scale self-assembly phenomena. Williams and Lísal developed CG models for graphene and GO in aqueous media using Martini water and a 4:1 mapping scheme.<sup>105</sup> Their simulations reproduced aggregation free energies in good agreement with experiments and revealed that GO dispersion is stabilized by electrostatic repulsion from surface functional groups, while pristine graphene aggregates *via*  $\pi$ – $\pi$  stacking. Poorsargol *et al.* performed combined experimental and MD simulations to study surfactant mixtures interacting with graphene sheets. Their results demonstrated that sodium dodecyl sulfate (SDS)-rich mixtures adsorb and self-assemble into monolayer and hemispherical structures, increasing surface charge and colloidal stability. Potential of mean force analysis confirmed enhanced repulsion and dispersion stability under higher surfactant coverage.<sup>111</sup> SDS molecules preferentially adsorbed at graphene edges, increasing the local density and altering solvent structuring, which improved colloidal stability. This highlights the ability of surfactants to modify interfacial energies and stabilize carbon nanomaterials.

Min *et al.* employed DPD simulations to investigate the self-assembly of CG graphene nanosheets (CGNS) with CG SDS(CSDS) surfactants in water (Fig. 11). The CGNS model, calibrated with bond stretch and angle-bend constants to maintain graphene's two-dimensional honeycomb structure, captured the dynamic adsorption process and equilibrium morphologies of surfactant-covered graphene. The simulations revealed that CSDS molecules initially adsorb along graphene edges, aligning parallel to the basal plane to minimize hydrophobic tail group exposure. As adsorption progressed, higher surfactant concentrations led to oversaturation at the edges, with additional molecules aggregating near the surface rather than forming multilayers. Micellar collapse onto graphene was more efficient at the edges than on the basal plane, due to reduced drag effects and enhanced penetration. Quantitative analysis of phase separation using order parameters confirmed that adsorption stabilized within  $\sim 47$  ns on average. Morphological evaluations showed that surfactants near the CGNS edges were oriented differently from those in the central region, emphasizing the critical role of edge effects in adsorption dynamics.<sup>37</sup>

Understanding graphene's interactions with solvents and amphiphilic molecules is critical for applications such as drug delivery, biosensing, and nanofluidics. Keshtkar *et al.* used DPD simulations to investigate the self-assembly of dipalmitoylphosphatidylcholine (DPPC) lipid molecules on carbon nanotubes (CNTs), offering insights translatable to graphene-based systems (Fig. 12).<sup>112</sup> Their study revealed a two-step self-assembly process: (1) an initial densification phase, where lipid molecules reorient to form an ordered monolayer, followed by (2) the formation of stable, densely packed structures influenced by CNT curvature. Higher curvature increased lipid surface density, which is crucial for designing biocompatible nanocarriers and can serve as a model for surfactant-assisted dispersion of graphene. The adsorption dynamics and ordering behavior observed here parallel molecular interactions with graphene surfaces, shedding light on how functional coatings or lipids stabilize carbon nanostructures in aqueous environments.

Wu *et al.* developed a CG MD model of PEO adsorption on graphene, demonstrating morphology transitions from patchy hemimicelles to edge-adsorbed monolayers as chain length and sheet size increased. While powerful, their model used a single CG mapping without explicit ionic strength or pH effects, limiting its predictive power in real-world aqueous systems.<sup>109</sup> Later studies, such as Poorsargol *et al.* expanded on this by incorporating surfactant mix dynamics and potential of mean force analysis to better model electrostatic stabilization and dispersion behavior.<sup>111</sup> Williams *et al.* conducted high-throughput MD simulations to quantify ion free-energy barriers in GO membranes, revealing how hydration-induced dehydration effects and pore non-uniformity influence ionic adsorption and interlayer structuring. Their findings underscore how surface oxidation and pore topology can dictate nanoscale assembly behavior in GO systems.<sup>113</sup>



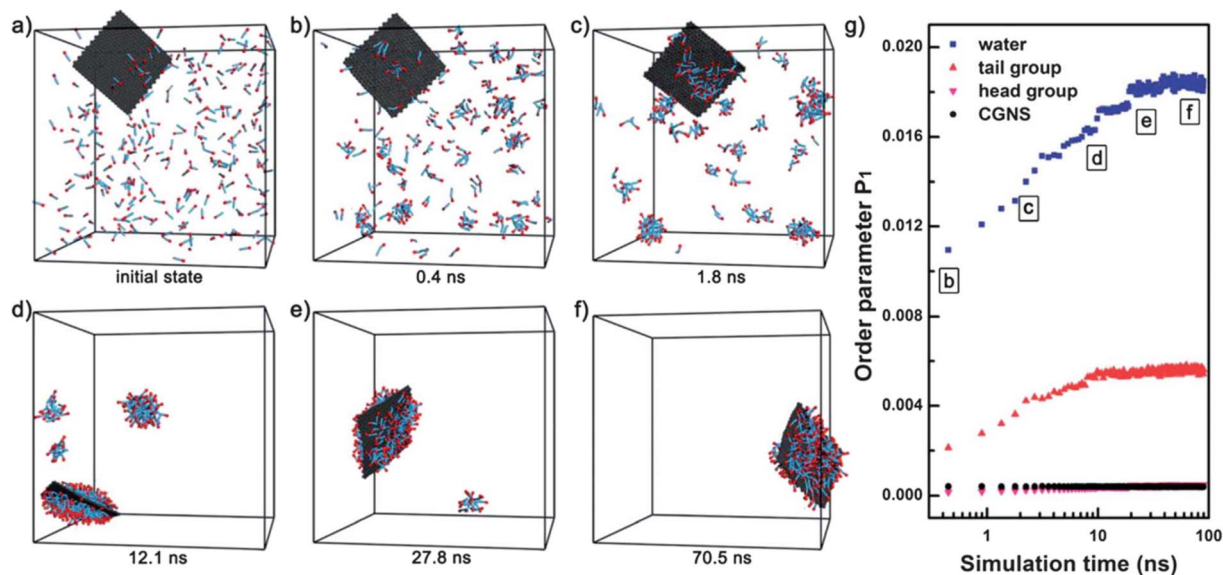


**Fig. 11** (a–f) Self-assembly sequence of CG graphene nanosheets (CGNS) with CSDS beads in water, illustrating adsorption dynamics and edge-induced micelle formation. (g) Evolution of the order parameter  $P1_{P1}$  for each bead type in the CGNS/CSDS system, calculated at intervals of 5000 simulation steps,<sup>37</sup> Used with permission of The Royal Society of Chemistry, from "Dissipative particle dynamics modeling of a graphene nanosheet and its self-assembly with surfactant molecules" by Sa Hoon Min, Choonghyeon Lee & Jyongsik Jang, *Soft Matter*, vol. 8, pp. 8735–8742, 2012; permission conveyed through Copyright Clearance Center, Inc.

#### 4.2. Interlayer and interfacial interactions

Understanding the interlayer and interfacial interactions in GO and related nanomaterials is crucial for tailoring their performance in composites, membranes, and energy devices. Several studies have combined atomistic, CG, and continuum approaches to model these complex phenomena. Dyer *et al.* developed an atomistic-continuum model based on the Lerf-Klinowski structural framework to investigate interaction forces

between GO sheets (Fig. 13).<sup>114</sup> By incorporating van der Waals and electrostatic forces through Lennard-Jones and Coulomb potentials, their model efficiently calculates interaction energies while maintaining good agreement with MD results. The study demonstrated that variations in oxidation and hydration levels strongly influence interlayer distance and binding energy. Higher oxidation levels increased both interlayer spacing and binding energy, while intercalated water molecules led to stepwise spacing increases due to hydrogen bonding. This

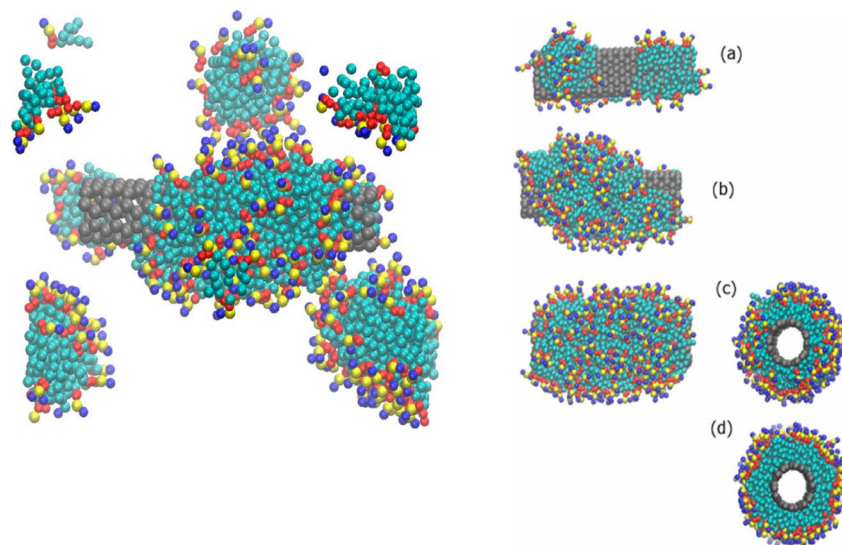


**Fig. 12** Left: Snapshot of DPPC in solution showing monomers and clusters adsorbing onto a (14, 14) CNT (water omitted). Right: Snapshots showing DPPC ordering around a (20, 20) CNT at different surface densities: (a) 0.28, (b) 0.83, (c) 1.05, and (d) 1.22 (corresponding to 0.56, 1.64, 2.09, and 2.43 nm<sup>-2</sup>, respectively), showing increased packing with higher coverage.<sup>112</sup> Adapted from *Nanomaterials*, 12(15), Mahboube Keshtkar, Nargess Mehdipour, Hossein Eslami, "Supramolecular self-assembly of dipalmitoylphosphatidylcholine and carbon nanotubes: a dissipative particle dynamics simulation study", 2022, Article 2653, licensed under CC BY 4.0.



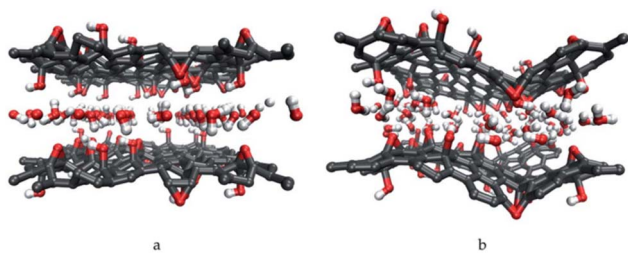


Fig. 13 (a) Configuration of a pair of 2 nm  $\times$  2 nm periodic GO sheets with intercalated water molecules after energy minimization. (b) Final structure of the same system after a 1000 ps MD simulation.<sup>114</sup> Used with permission of The Royal Society of Chemistry, from "Modelling the interaction of graphene oxide using an atomistic-continuum model" by T. Dyer, N. Thamwattana & R. Jalili, *RSC Adv.*, vol. 5, pp. 77062–77070, 2015; permission conveyed through Copyright Clearance Center, Inc.

analytical model significantly reduces computational cost compared to fully atomistic simulations, making it practical for large-scale GO studies, while still capturing key physical trends observed experimentally.

Building on this, Shang *et al.* used atomistic simulations to explore the energetics and alignment behavior of GO nanosheet assemblies. Their study incorporated force fields calibrated using first-principles calculations, enabling an accurate depiction of the potential energy surface governing interfacial interactions.<sup>40</sup> They systematically varied the degree of oxidation, sheet misalignment, and water content, revealing that partial oxidation leads to anisotropic charge distributions, which promote edge-to-face stacking geometries. Their findings offered molecular-level understanding of how functional group heterogeneity influences stacking orientation, with implications for stability and dispersion behavior in polar solvents.

More recent CG and CG-DPD models have extended this understanding to mesoscale dynamics. These models incorporate effective potential for polar and nonpolar interactions, enabling simulation of large ensembles of GO sheets in ionic or humid environments. Studies have shown that multivalent ions such as  $\text{Ca}^{2+}$  and  $\text{Mg}^{2+}$  compress the electrical double layer (EDL) and reduce hydration repulsion, causing GO lamellae to collapse and aggregate. In contrast, monovalent ions and surfactant molecules can expand interlayer spacing by enhancing hydration and introducing steric barriers. For example, simulations using the Martini force field with explicit solvent show reversible swelling behavior in response to relative humidity changes, with interlayer spacing modulating from  $\sim 0.8$  nm (dry) to over 1.2 nm (humid conditions). These results align with experimental SAXS and AFM data and highlight the importance of solvent structure and ionic strength in designing GO-based membranes and dispersions.

Recent atomistic MD simulations have also quantified how GO hydration and oxidation impact nanoscale structure. Devanathan *et al.* demonstrated that as GO hydrates, interlayer spacing increases from  $\sim 0.8$  nm to  $\sim 1.1$  nm, while water diffusion is slowed by strong hydrogen bonding. These results were consistent with neutron scattering experiments and showed the importance of solvent-structured layers in limiting

molecular mobility.<sup>115</sup> *Ab initio* MD by Mouhat *et al.* highlighted clustering of epoxide/hydroxyl groups on GO surfaces and quantified a negative surface charge of  $\sim -10$  mC  $\text{m}^{-2}$  in water, underscoring GO's dynamic chemical and structural response upon hydration.<sup>116</sup> Overall, simulation studies have clarified that interfacial interactions in GO systems are governed by a subtle interplay of van der Waals forces, electrostatics, hydration effects, and surface chemistry. Future directions include machine learning-guided force field refinement, explicit pH-dependent protonation modeling, and multiscale coupling of atomistic and continuum models to better predict dynamic stacking behavior under flow or confinement conditions relevant to water purification, nanofluidics, and layered nanocomposites.

#### 4.3. Carbon nanotube-polymer systems

The dispersion and alignment of CNTs in polymer matrices are critical to the mechanical, thermal, and electrical performance of nanocomposites. Molecular simulations, particularly DPD, CG-MD, and atomistic MD, have been instrumental in elucidating the mechanisms governing CNT-polymer interactions. Zhou *et al.* studied CNT dispersion and alignment in polymer matrices using DPD simulations.<sup>117</sup> They showed that dispersion stability depends on matrix viscosity, shear flow, and CNT aspect ratio. Under flow, CNTs aligned preferentially along the velocity gradient, a behavior beneficial for enhancing the mechanical performance of nanocomposites. Further insights have been provided by Chawla and Sharma<sup>118</sup> who used atomistic MD simulations to investigate CNT pull-out behavior from a polyethylene matrix. They modeled a single-walled (5, 5) CNT embedded within an amorphous PE system and applied quasi-static axial displacement to the CNT. The simulation captured interfacial shear stress as a function of displacement and quantified pull-out energy. Their results showed that van der Waals interactions and polymer chain entanglement were the dominant contributors to interfacial shear strength. The study also evaluated the influence of polymer chain length and CNT embedment length on load transfer efficiency, providing a detailed force–displacement relationship. To simulate larger systems, Hente *et al.* employed a CG-MD model to simulate the mechanical behavior of CNT-reinforced PMMA composites. Their model included short CNTs dispersed in a cross-linked PMMA matrix with tunable interaction parameters.<sup>119</sup> The simulations varied CNT volume fraction and degree of interfacial cross-linking to examine the resulting elastic modulus. The study showed that higher CNT loading and increased cross-link density significantly improved stiffness, with results closely matching continuum micromechanics models and full atomistic benchmarks. This CG approach enabled simulations of larger systems while preserving essential interfacial mechanics. Recent CG-MD simulations have further detailed how polymer grafting and volume fraction influence CNT dispersion and mechanical reinforcement.

Ileri-Ercan *et al.* used Martini-3 CG simulations of polystyrene-functionalized CNTs in lipid bilayers to quantify how grafting density controls alignment and membrane



deformation, highlighting parallels between polymer and bio membrane interactions.<sup>120</sup> Arash, Park & Rabczuk applied a CG model to CNT/polymer nanocomposites, demonstrating a direct scaling of composite Young's modulus with CNT volume fraction and validating the approach against atomistic results.<sup>63</sup> Collectively, these simulations offer predictive capabilities for optimizing CNT-polymer nanocomposites. By evaluating interfacial energetics, dispersion quality, and alignment behavior, molecular models help bridge nanoscale interactions with macroscale processing outcomes. This understanding is vital for designing mechanically robust, thermally conductive, and electrically active polymer nanocomposites.

## 5. Defects

Defects play a pivotal role in determining the mechanical, electrical, and thermal properties of graphene and related carbon nanostructures. While pristine graphene exhibits exceptional strength and conductivity, real-world applications inevitably involve intrinsic and extrinsic defects that alter its performance. Molecular simulations have proven essential in understanding how different types of defects ranging from point vacancies and substitutional dopants to extended topological irregularities like SW defects and grain boundaries influence material behavior. Recent studies highlight the dual role of defects in graphene: while intrinsic point and line defects can degrade electronic and mechanical properties, they also offer opportunities for tailoring local functionalities. Graphene uniquely reconstructs its lattice around vacancies and line defects, stabilizing divacancies and enabling novel electronic behaviors. Extrinsic defects, such as dopant atoms, can strongly modulate charge distribution, band structure, and induce phenomena like magnetism or Kondo effect. Controlled introduction of such defects is thus crucial for designing graphene-based devices with targeted properties.<sup>121</sup>

Atomistic MD simulations have been widely used to probe defect-induced mechanical failure in graphene. Studies have shown that vacancies and SW defects can serve as nucleation sites for crack propagation and drastically reduce tensile strength. Ho *et al.* demonstrated through atomistic MD that single vacancy defects in graphene nanoresonators lead to localized stiffness degradation, which in turn lowers the resonant frequency and quality factor (*Q*-factor), highlighting the influence of atomic vacancies on both mechanical and dynamic stability.<sup>122</sup> For instance, Juneja and Rajasekaran performed MD simulations of graphene sheets containing Stone–Thrower–Wales (STW) defects under uniaxial strain and observed anomalous strength characteristics, including bond rotation, local lattice distortion, and fracture stress reduction. Their study showed that STW defects not only serve as crack initiation sites but also alter out-of-plane deformation patterns and energy dissipation mechanisms.<sup>123</sup> Such defects lead to localized stress concentrations and significantly impact crack initiation and propagation paths. In contrast, certain configurations of defects can enhance fracture toughness by promoting distributed damage and energy dissipation.

Defect engineering emerges as a powerful strategy for enhancing the mechanical resilience of graphene, as demonstrated by the role of STW defects in improving fracture toughness. Using MD simulations, recent studies highlight how these defects, formed by rotating carbon–carbon bonds, redistribute stress and induce out-of-plane displacements near crack edges, significantly boosting graphene's fracture resistance. For pristine graphene, carefully positioned STW1 defects enhance fracture toughness by up to 28%, while in hydrogenated graphene, partially hydrogenated structures outperform fully hydrogenated ones due to the stability provided by mixed  $sp^2$  and  $sp^3$  hybridization states. The simulations, employing the AIREBO potential, show that STW defects effectively suppress crack-tip stress, facilitate atomic chain bridging, and counteract hydrogen-induced distortions. These findings emphasize the potential of STW defects in tailoring graphene's mechanical properties, offering critical insights for designing durable graphene-based materials in various applications.<sup>124</sup>

To overcome the limitations of atomistic scale, CG models have been developed to simulate large-scale fracture phenomena in defective graphene. Mohammadi *et al.* developed a CG MD framework to study the mechanical and thermal properties of defective carbon nanomaterials, including graphene. Their model incorporated vacancy defects distributed across graphene sheets and was calibrated against full atomistic simulations to ensure accuracy in predicting stress–strain responses and thermal transport.<sup>125</sup> The simulations revealed how defect density influenced crack branching, fracture patterns, and localized failure mechanisms in extended graphene sheets. These models allow for system sizes spanning hundreds of nanometers, making them suitable for predicting mechanical behavior in real-world device geometries.

More recently, machine learning (ML) approaches have emerged as a powerful complement to traditional simulations. Data-driven models trained on MD-generated datasets can rapidly predict defect-induced changes in elastic modulus, fracture strength, or thermal conductivity across a wide parameter space. For example, Recent work has applied convolutional neural networks (CNNs) to analyze MD datasets of defect-laden graphene and predict mechanical properties such as fracture stress. For instance, deep CNN architectures have been trained to recognize defect geometries and classify their impact on fracture energy distribution, enabling rapid screening of failure-prone configurations, while Gupta *et al.* employed graph neural networks (GNNs) to model atom-level failure behavior based on structural topology.<sup>126</sup>

Together, these simulation strategies offer multiscale insight into defect-driven behavior in graphene systems. One particularly important direction is the study of disclinations in polycrystalline graphene Fig. 14. Romanov *et al.* (2018) reviewed the atomic configurations of improper carbon rings, such as 5-7, 5-8-5, and 555-777, and used both MD simulations and elastic theory to model grain boundaries and pseudo-graphenes. Their simulations revealed that disclination arrangements such as quadrupoles significantly influence the energy, stability, and structure of grain boundaries Fig. 15. The study further demonstrated how symmetric and asymmetric grain



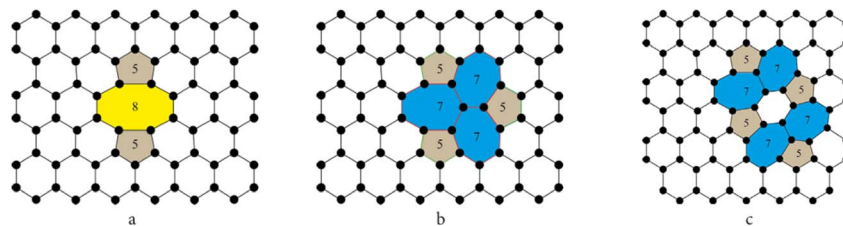


Fig. 14 Representative atomic structures of disclination defects in graphene, including (a) 5-8-5, (b) 555-777, (c) 5555-7777 complexes. These topological irregularities alter lattice symmetry, introduce local curvature, and contribute to the formation of grain boundaries.<sup>127</sup> Adapted from *Letters on Materials*, 8(4), A. E. Romanov, M. A. Rozhkov, A. L. Kolesnikova & I. S. Yasnikov, "Disclinations in polycrystalline graphene and pseudo-graphenes", pp. 384–400, licensed under CC BY.

boundaries, characterized by different distributions of 5-, 7-, and 8-membered rings, exhibit energy variations from 0.4 to over  $2 \text{ eV } \text{Å}^{-1}$ .<sup>127</sup>

These results enhance our understanding of how microstructural features at the atomic scale control macroscopic mechanical behavior, supporting the development of graphene defect engineering. MD provides atomic-level resolution, CG approaches extend to device-relevant scales, and ML enables rapid screening and surrogate prediction. However, challenges remain in integrating these methods coherently and validating predictions against experimental data. Future work should focus on developing hybrid multiscale workflows that combine accuracy, efficiency, and data robustness for modeling real-world defective graphene systems. Chemical functionalization and defect engineering are inherently interconnected approaches that strategically introduce or modify structural imperfections at the atomic level, allowing tailored control of graphene's properties. Unlike intrinsic structural defects such as vacancies and dislocations, chemically induced defects involve precise atomic or molecular alterations that influence mechanical, thermal, and electronic characteristics.

Chemical functionalization techniques like hydrogenation, oxidation, fluorination, and atomic doping systematically introduce defects that alter graphene's pristine structure. Pei *et al.* utilized reactive MD simulations to show how hydrogenation transforms robust  $\text{sp}^2$  bonds into weaker  $\text{sp}^3$  hybridizations, creating local structural defects that degrade tensile strength by around 65% at partial hydrogenation.<sup>47</sup> Ruiz *et al.* extended this analysis using CG modeling, demonstrating that hydrogenation-induced defects significantly lower graphene's

Young's modulus and substantially alter its deformation mechanisms.<sup>38</sup> Atomistic simulations of oxidation processes leading to GO and rGO have revealed detailed insights into defect formation driven by oxygen-containing functional groups. Shang *et al.* performed comprehensive atomistic simulations illustrating how epoxide and hydroxyl groups induce defects, expanding interlayer spacing and significantly modifying thermal and mechanical behaviors.<sup>40</sup>

Kumar *et al.* demonstrated *via* density functional theory (DFT)-informed simulations how oxidation enhances defect densities, thereby substantially altering electronic properties and chemical reactivity.<sup>128</sup> Additionally, fluorination studies combining MD and DFT simulations revealed that fluorine atoms create localized  $\text{sp}^3$  defect sites, influencing mechanical and electronic characteristics.<sup>129</sup> The synergy between chemically induced defects and existing structural defects profoundly impacts graphene's performance. Juneja and Rajasekaran, using detailed MD simulations, revealed that STW defects redistribute local stress fields, influencing fracture toughness and dynamics significantly when combined with adjacent chemically functionalized regions.<sup>4,123</sup> The simulations elucidated mechanisms such as defect-induced crack bridging and altered fracture pathways. Mohammadi *et al.* employed an energy-based CG simulation framework to elucidate how chemically functionalized defects interact with intrinsic structural defects, collectively influencing fracture propagation, local stiffness, and thermal conductivity. Their simulations explicitly accounted for varying defect densities and chemical environments, highlighting the combined roles of structural and

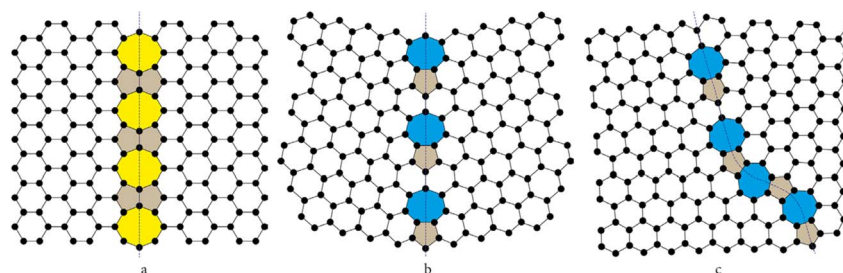


Fig. 15 Grain boundary energy as a function of misorientation angle for various disclination configurations in graphene chain of (a) 5-8-5 carbon rings, (b) symmetric, and (c) nonsymmetric grain boundaries. The plot highlights energy differences between symmetric and asymmetric boundaries, derived from MD simulations and elastic theory.<sup>127</sup> Adapted from *Letters on Materials*, 8(4), A. E. Romanov, M. A. Rozhkov, A. L. Kolesnikova & I. S. Yasnikov, "Disclinations in polycrystalline graphene and pseudo-graphenes", pp. 384–400, licensed under CC BY.



chemical modifications in controlling mechanical robustness and thermal performance.<sup>125</sup>

Graphene functionalization critically influences the formation and evolution of interfacial defects in composite materials; a phenomenon rigorously explored *via* multiscale simulations. Lin *et al.* combined DPD simulations with finite element modeling (FEM) to analyze the dispersion of polymer-functionalized graphene sheets (PMMA@FGN). Their simulations showed that functionalization significantly reduced interfacial defects, enhanced dispersion stability, and consequently improved the mechanical properties and reliability of the graphene–polymer composite system.<sup>65</sup> Liba *et al.* applied DPD modeling to investigate surfactant-functionalized carbon nanotube (CNT) dispersion within polymer matrices, highlighting improved stability and fewer interfacial defects. Their findings illustrate how surface functionalization simulations can guide effective defect control and optimization of interfacial properties critical for composite fabrication.<sup>54</sup>

Advances in ML methods have significantly enhanced the ability to predict complex functionalization-defect interactions efficiently. Zheng *et al.* leveraged high-throughput MD simulations and neural networks to rapidly predict mechanical and thermal property changes resulting from functionalization-induced defects. This ML approach enables swift screening and optimization of chemically functionalized graphene structures.<sup>130</sup> Gupta *et al.* implemented GNNs to simulate detailed atomic-level interactions between chemical groups and graphene defects, providing precise predictions of resulting mechanical behaviors. Such computational frameworks significantly streamline the exploration of the functionalization-defect landscape, facilitating the identification of optimal graphene modifications.<sup>126</sup> Understanding the evolution, dynamics, and stability of defects in graphene is crucial for predicting its mechanical, thermal, and electronic behaviors under practical operational conditions. Computational methods, particularly MD, kinetic Monte Carlo (kMC), and DFT, provide detailed insights into defect mechanisms, pathways, and stability criteria.

Defects in graphene, such as vacancies and STW defects, originate and evolve through specific atomic mechanisms. Reactive MD simulations have revealed vacancy migration pathways and the critical role of mechanical strain in enhancing vacancy mobility. For instance, recent simulations demonstrate significant room-temperature vacancy diffusion under moderate tensile strain conditions (~0.8%), highlighting strain-driven defect dynamics.<sup>131</sup> Furthermore, combined MD and kMC studies offer insights into long-term vacancy evolution, showing complex coalescence and spatial clustering patterns over extended timescales and large graphene areas.<sup>132</sup> Temperature and mechanical strain profoundly influence defect behavior. MD analyses have demonstrated how temperature variations and tensile loading affect defect-induced vibrational properties, altering graphene's dynamical response and mechanical stability.<sup>133</sup> Additionally, strain-induced mobility studies indicate that mechanical deformation significantly accelerates vacancy migration and clustering, which can

substantially impact graphene's durability and operational performance.<sup>131</sup>

Defect clustering significantly modifies graphene's mechanical, thermal, and electronic properties. Computational studies tracking vacancies *via* kMC and MD methods reveal clustering behaviors, illustrating how vacancy concentrations affect graphene's structural integrity and transport properties.<sup>132</sup> These studies emphasize the necessity of controlling defect densities to maintain desired graphene functionalities in practical applications. Advanced simulation methodologies such as kMC and accelerated MD enable investigations into defect dynamics beyond conventional MD timescales. Recent large-scale kMC simulations of graphene growth and etching effectively model defect generation, healing processes, and evolution at edges and during substrate interactions, offering crucial insights into defect management strategies.<sup>132,134</sup> Substrates and environmental conditions significantly impact defect formation and stability. Atomistic MD simulations illustrate how substrates influence the healing of topological defects, such as pentagonal disclinations (“scars”), through modifications in local coordination and bonding structures.<sup>135</sup> Additionally, quantum-mechanical MD simulations capture environmental interactions, revealing how graphene vacancies interact dynamically with water, either promoting vacancy healing or stabilizing defect structures, depending on hydration conditions.<sup>136</sup>

Machine learning (ML) techniques trained on MD- and DFT-derived data sets represent a powerful approach to predicting defective evolution pathways efficiently. ML-driven predictions accelerate defect simulations and offer valuable guidance for long-term behavior forecasting, thus significantly enhancing computational efficiency and predictive accuracy for practical graphene applications. Defects in graphene, ranging from point defects to grain boundaries and functionalized sites, substantially modulate their physical properties. Advanced simulations have become instrumental in dissecting these effects, allowing quantitative predictions across thermal, mechanical, electronic, and chemical domains. Reactive MD simulations have investigated fracture behavior in defective graphene under tensile loading, demonstrating that intrinsic defects significantly alter crack propagation paths and strength reductions.<sup>137</sup> A reactive MD study by Liu *et al.* demonstrated how vacancy clusters influence crack initiation and propagation, highlighting the importance of defect distribution in determining fracture modes.<sup>138</sup>

A CNN-guided NEMD study revealed that structural disorder and defects in multilayer graphene induce pronounced reductions in thermal conductivity, up to ~60%.<sup>139</sup> Additional NEMD simulations confirm that both vacancy shape and concentration dramatically increase phonon scattering.<sup>94</sup> DFT analysis of out-of-plane defects revealed modulation of electron transmission through quantum interference effects.<sup>140</sup> A tight-binding study showed how edge notches in graphene nanoribbons create localized states and impact transport behavior.<sup>141</sup> Recent DFT work detailed O<sub>2</sub> adsorption at vacancy sites on graphene, showing enhanced energetics and potential catalytic applications.<sup>142</sup> MD and DFT simulations at graphene–copper



interfaces highlighted how defect-driven phonon scattering and interfacial chemistry influence composite performance.<sup>143</sup>

## 6. Incorporating machine learning in graphene simulations

Machine learning (ML) has emerged as a transformative tool for accelerating and extending the capabilities of computational simulations related to graphene. From predicting atomic-scale defects to optimizing functional properties and discovering new materials, ML techniques are being widely integrated with classical and quantum mechanical simulations, including MD, DFT, and kMC methods.

### 6.1. Machine learning for defect prediction and formation pathways

Machine learning-based techniques have achieved atomic-level precision in detecting and classifying defects in graphene. Zheng and Gu developed a machine learning framework using kernel ridge regression trained on thermal vibration data extracted from MD simulations. They implemented two distinct workflows: an atom-based approach, which evaluates local displacement features per atom, and a domain-based approach, which averages data over spatial patches of the graphene sheet. These workflows enabled robust detection and classification of vacancy and topological defects with approximately 90% accuracy, even without prior specification of defect type. Their

framework distinguishes between atom-based and domain-based ML workflows, both of which are visualized in Fig. 16.<sup>144</sup>

Zheng *et al.* further applied transfer learning techniques to generalize defect prediction from smaller MD models to larger graphene sheets, reaching up to 80% accuracy. These scalable methods reduce the computational burden associated with large-scale DFT defect mapping.

Supervised learning techniques, such as support vector machines (SVM), decision trees, and random forests (RF), have been employed to predict vacancy formation energies, migration barriers, and defect clustering tendencies in graphene. Yang and Buehler proposed a graph neural network framework for predicting defect-induced mechanical property changes in crystalline solids, including graphene. Although their model focuses primarily on GNNs, it establishes a foundational link between atomic-level defects and mesoscale mechanical behavior, offering insights comparable to supervised learning methods like SVMs for defect classification. Recent studies have leveraged GNNs to model the atomic connectivity of graphene, allowing accurate predictions of defect energetics and transition states under varying mechanical and thermal conditions.<sup>145</sup> For example, Xie and Grossman introduced a crystal graph convolutional neural network (CGCNN) that accurately predicts formation energies, including those related to defects, using atomic connectivity graphs derived from DFT datasets. Additionally, active learning frameworks have been developed to iteratively explore defect configuration space, reducing the number of *ab initio* calculations while improving model generalizability.<sup>146</sup>

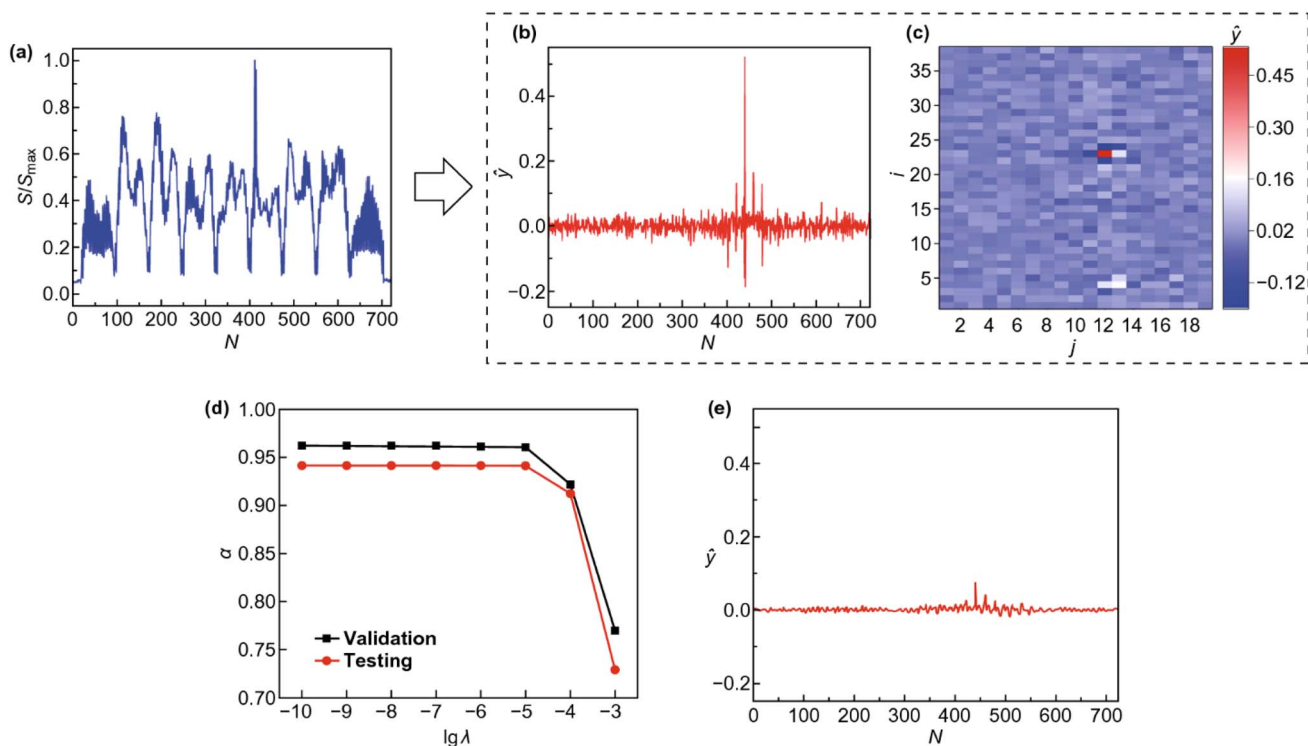


Fig. 16 Atom-based machine learning prediction of a single-atom vacancy in graphene. (a) Example of the input energy vector from MD simulations. (b) Predicted label vector indicating defect presence. (c) 2D spatial map showing predicted defect intensity. (d) Validation and testing accuracy vs. regularization parameter  $\lambda$ . (e) Label vector output under strong regularization.<sup>144</sup> Reproduced from "Machine learning-based detection of graphene defects with atomic precision" by Bowen Zheng and Grace X. Gu, *Nano-Micro Letters*, 12:181 (2020), CC BY 4.0.



In addition to deep learning and graph-based models, ensemble machine learning frameworks have also shown promise for defect modeling. Chen *et al.* developed an ensemble approach to train interatomic potentials that generalized across different atomic environments, including defective graphene. Their method integrated a variety of descriptors and model types to improve robustness and reduce overfitting, facilitating accurate predictions of force fields in heterogeneous systems.<sup>147</sup> Jha *et al.* extended this methodology to the electronic domain, using RF regression on high-throughput DFT datasets to predict electronic band gaps in functionalized and defective graphene materials. These studies underscore the broader versatility of supervised learning models, not only for structural predictions but also for electronic property estimation, highlighting their value in multiscale simulations where defects substantially influence local and global graphene behavior.<sup>148</sup>

Zuo *et al.* conducted a comprehensive benchmarking study of machine-learned interatomic potentials (MLIPs), such as SNAP, GAP, and ANI, to assess their accuracy and robustness in modeling defect structures, migration energies, and stress distributions in various materials, including graphene. Their findings showed that MLIPs trained on high-quality DFT datasets can achieve near-DFT accuracy in predicting formation energies and elastic properties of defective graphene, while offering orders-of-magnitude speedup over *ab initio* calculations.<sup>149</sup> This work highlights the importance of training diversity and model selection in MLIP development for reliable simulation of defective 2D materials.

## 6.2. ML-accelerated MD and predictive force field surrogates

Machine-learned force fields (MLFFs) and surrogate models have become essential tools in overcoming the limitations of traditional quantum mechanical methods for simulating large-scale graphene systems. By learning interatomic potentials directly from high-fidelity quantum data, these models can replicate *ab initio* accuracy with dramatically reduced computational cost, enabling dynamic simulations of thousands of atoms over extended time scales. Among the most impactful advancements in molecular simulations of graphene is the Deep Potential Molecular Dynamics (DeePMD) framework, which employs deep neural networks to represent potential energy surfaces with *ab initio* accuracy. Trained on DFT data, DeePMD models have replicated key physical properties of pristine and defective graphene, including phonon dispersion curves, thermal conductivity, and mechanical behavior, with remarkable precision. Lu *et al.* (2021) demonstrated that DeePMD enables large-scale simulations of up to 100 million atoms, capturing phenomena such as fracture initiation, crack propagation, dislocation dynamics, and phonon transport at resolutions unattainable by traditional DFT or tight-binding methods. Their work also introduced efficient training protocols using force-matching and energy consistency, enhancing the model's transferability across diverse graphene-based systems. This breakthrough allows mesoscopic modeling and lifetime prediction of nanodevices under thermal and

mechanical stress, bridging the gap between quantum accuracy and classical scale.<sup>150</sup>

In addition to DeePMD, recent advances have introduced equivariant neural network models such as NequIP, which explicitly enforce physical symmetries, including rotational and translational invariance through SE(3) equivariance. These architectures significantly enhance data efficiency, transferability, and generalizability in machine-learned force fields (MLFFs). Although NequIP has not yet been specifically applied to graphene, it has demonstrated exceptional performance across a variety of material systems, particularly in capturing interatomic forces, stress fields, and symmetry-breaking phenomena in structurally complex regions such as grain boundaries and defect dipoles. Batzner *et al.* showed that NequIP could extrapolate to previously unseen configurations, maintaining accurate force predictions across temperatures and defect landscapes.<sup>151</sup> Its ability to resolve subtle stress localizations and variations in elastic properties suggests strong potential for modeling defect-laden graphene and other two-dimensional materials, where traditional force fields often fall short.

Another influential model, SchNet, developed by Schütt *et al.* is a continuous-filter convolutional neural network that achieves chemical accuracy in predicting energies and forces for a wide range of systems. SchNet, originally developed for molecular systems, has been extended to periodic and 2D materials, including carbon-based systems. Its adaptability suggests strong potential for modeling functionalized graphene and GO, especially for predicting vibrational spectra and binding energies, although direct applications remain limited. It accurately predicts binding energies, vibrational spectra, and interfacial adhesion with DFT-like precision. Its capacity to model structural distortions and functional group effects suggests strong potential for accelerating the screening of thermodynamic and vibrational properties in graphene-based systems.<sup>152</sup> Furthermore, when integrated with active learning loops, SchNet can refine its predictive accuracy on-the-fly by selecting new, informative configurations, making it highly suitable for chemically diverse and dynamic environments.

## 6.3. Electronic, thermal, and mechanical property prediction

Machine learning (ML) has been extensively used in cheminformatics to predict binding affinities,<sup>153</sup> aqueous solubilities,<sup>154–156</sup> partition coefficients,<sup>157</sup> and other physicochemical properties.<sup>158</sup> These successes illustrate the versatility of ML in capturing complex structure–property relationships. Leveraging these methodologies, researchers have increasingly applied ML to graphene and related nanomaterials, integrating it with MD and DFT to accelerate the prediction of key electronic, thermal, and mechanical properties. This synergy allows for rapid screening, optimization, and design of graphene-based systems with reduced computational cost. ML models are increasingly used to predict electronic, thermal, and mechanical properties of graphene systems, complementing traditional MD and DFT simulations by offering faster and scalable approaches.



**6.3.1. Electronic properties.** Recent advances have extended ML applications beyond band gap prediction to detailed electronic structure analyses. SVM, RF, and deep neural networks (DNNs) are increasingly employed to predict band structures, Fermi levels, and defect-related states in pristine, doped, and functionalized graphene. Jha *et al.* demonstrated that RF models trained on high-throughput DFT data can accurately predict band gaps for chemically modified graphene derivatives.<sup>148</sup> Moreover, Xie and Grossman introduced the Crystal Graph Convolutional Neural Network (CGCNN), which has been successfully applied to model electronic density of state and defect-induced states.<sup>146</sup>

**6.3.2. Thermal properties.** Advanced ML models are now widely used to predict thermal conductivity, phonon transport, and heat capacity in graphene systems. A recent study by Chen *et al.* introduced a unified deep learning framework that integrates convolutional neural networks (CNNs) with physics-informed layers to model interlayer phonon coupling and cross-plane heat transport in bilayer graphene and h-BN heterostructures. Their model effectively accounts for stacking orders, interlayer van der Waals interactions, and temperature dependence, achieving predictive errors below 3% compared to direct Boltzmann transport equation calculations while reducing computational time by two orders of magnitude.<sup>159</sup> Similarly, Li *et al.* developed a hybrid deep learning architecture that combines GNNs with transfer learning to analyze thermal conductivity across a range of stacking configurations, defect densities, and functionalization levels. Their model incorporates descriptors derived from both atomic topology and phonon spectra, enabling accurate prediction of both in-plane and cross-plane thermal conductivity.<sup>77</sup> The framework also demonstrated predictive capability for thermal boundary resistance in graphene/BN heterostructures, making it applicable to real-world device designs.

Other ML-driven frameworks, such as Gaussian process regression (GPR), kernel ridge regression (KRR), and neural network potentials (NNPs), have been applied to predict phonon lifetimes, specific heat, and anharmonic effects in large-scale simulations. ML-based inverse design approaches also enable the optimization of isotopic compositions or defect patterns to achieve targeted thermal conductivities, which is particularly relevant for applications like thermoelectric devices and thermal management in flexible electronics.

**6.3.3. Mechanical properties.** High-throughput MD simulations coupled with ML models such as artificial neural networks (ANNs) and GPR have been used to predict Young's modulus, fracture strength, and tensile failure. Gupta *et al.* applied a sparse ML framework based on D-optimal design to explore mechanical responses of graphene under strain, incorporating defect density, doping, and strain rate as input features. Their approach reduced the computational cost by an order of magnitude while maintaining accuracy above 95% compared to direct MD results.<sup>126</sup> Zhang *et al.* demonstrated a novel approach by integrating ML algorithms with high-throughput MD simulations to study temperature, strain rate, vacancy defects, and chirality effects on fracture strain, fracture

strength, and Young's modulus Fig. 17. They tested models including k-nearest neighbors (KNN), SVM, decision trees (DT), and ANNs, finding that ANNs delivered the most accurate predictions. Results indicated that temperature and vacancy defects reduce mechanical strength, while strain rate enhances it, with significant chirality-dependent variations. This framework allows for accurate predictions of mechanical properties within seconds, significantly reducing computational time.<sup>69</sup>

Predicting the mechanical properties of nanocomposites is a critical challenge in materials science due to the complex interactions between components, particularly under varying conditions of temperature, orientation, and composition. A hybrid approach combining MD simulations and ML, specifically long short-term memory (LSTM) models, has been employed to predict the nanoindentation hardness of nickel-graphene nanocomposites. MD simulations investigated how graphene volume fraction, orientation angles, and temperature influence mechanical performance. The LSTM model trained on force-depth data achieved a Pearson correlation coefficient above 0.95, outperforming traditional ML models such as SVM and MLP. This integration of MD and ML reduces computational time significantly, predicting mechanical properties in seconds *versus* hours for direct MD, highlighting the role of graphene's microstructural characteristics in determining composite behavior.<sup>160</sup>

Advancing the understanding of graphene's mechanical properties under defects and doping is critical for optimizing its applications. Another study integrates MD with ML using a D-optimal design algorithm to reduce computational costs without compromising accuracy. Five input features, temperature, strain rate, single vacancy defects, silicon doping, and edge effects, were varied to evaluate fracture strength, failure strain, and Young's modulus. Gaussian process regression (GPR) models showed superior predictive accuracy for complex

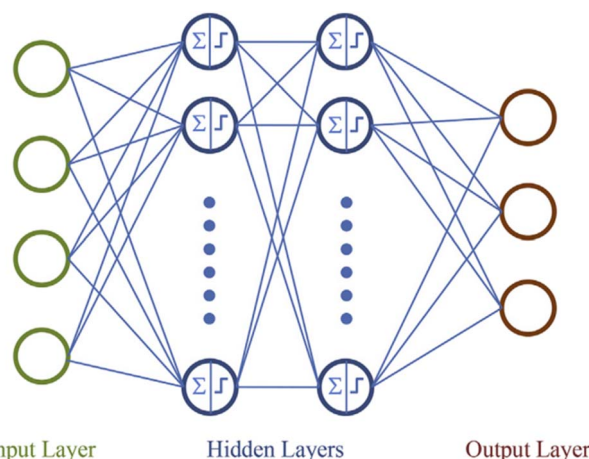


Fig. 17 Illustration of a standard neural network architecture featuring an input layer, two hidden layers, and an output layer.<sup>69</sup> Reprinted from *Carbon*, vol. 148, Zesheng Zhang, Yang Hong, Bo Hou, Zhongtao Zhang, Mehrdad Negahban & Jingchao Zhang, "Accelerated discoveries of mechanical properties of graphene using machine learning and high-throughput computation", pp. 115–123, Copyright 2019, with permission from Elsevier.



mechanical behavior, providing deeper insights into cross-dependencies among parameters and enabling efficient 2D material studies.<sup>126</sup> Another deep ML approach combines analytical quantized fracture mechanics, MD, and neural networks to study fracture strength under the influence of defects, crack orientation, and high temperatures. The deep ML model achieved high predictive accuracy (MAPE below 5%) using transfer learning, significantly reducing computational overhead while maintaining fidelity across conditions such as crack sizes, orientations, and lattice configurations.<sup>161</sup>

#### 6.4. Integrated frameworks

Recent studies have explored multitask learning frameworks that simultaneously predict mechanical, thermal, and electronic properties using shared descriptors such as temperature, strain, and chemical environment. This integrated approach allows for cross-property correlation analysis and faster optimization of graphene materials for applications in nanoelectronics, flexible devices, and thermal interface materials. Additionally, ML methods have been applied to optimize mechanical flexibility in graphene kirigami designs, where CNN-based inverse design strategies identify optimal cut configurations to maximize stretchability with minimal simulations, as shown by Hanakata *et al.* This iterative ML-guided design reduced the search space from millions of configurations to just hundreds, discovering highly stretchable patterns.<sup>162</sup>

Finally, ML-driven multiscale frameworks, like that developed by Khoei *et al.*, integrate atomistic MD with continuum finite element models using MLP-ANNs. These frameworks accurately predict nonlinear mechanical responses under tension, shear, torsion, and nano-indentation while eliminating predefined constitutive models and reducing computational costs. Such approaches are particularly relevant for graphene's nonlinear mechanical behavior.<sup>163</sup> These developments highlight the potential of ML-based predictive modeling in accelerating the design and discovery of advanced graphene-based materials.

#### 6.5. Advanced ML-driven design and predictive approaches

Beyond property prediction, ML is increasingly applied to complex tasks such as thermodynamic modeling, solvation analysis, and structural optimization. While ML has seen significant application in electronic and mechanical domains, its use in predicting thermodynamic and solvation properties for graphene-related systems remains underexplored. Traditional methods like Free Energy Perturbation (FEP), thermodynamic integration (TI), and linear interaction energy (LIE) models are computationally expensive. Recent work has introduced Molecular Dynamics Fingerprints (MDFP), which integrate statistical descriptors from MD data such as potential energy distributions, radius of gyration, and solvent-accessible surface area into ML models. These approaches provide accurate predictions of solvation free energies and partition coefficients at a fraction of the computational cost, opening avenues for studying graphene in solvents or composites.<sup>164</sup>

Another notable application involves the design of graphene-based metamaterials. Hanakata *et al.* used a CNN trained on

MD simulations to predict mechanical responses (yield strain and stress) of graphene kirigami structures based on cut density and placement. By exploring a design space of over 4 million possible patterns, their ML-guided inverse design approach identified optimal cut configurations, achieving enhanced stretchability and mechanical flexibility. Fig. 18 illustrates this ML-driven optimization process.<sup>162</sup>

While machine-learning force fields (ML-FFs) significantly extend the accessible time and length scales of molecular simulations, their predictive reliability is ultimately constrained by the quality, diversity, and representativeness of the reference data used for training. As emphasized in recent critical reviews, ML-FFs may exhibit excellent interpolation accuracy within the training domain but can suffer from uncontrolled extrapolation errors when applied to new chemistries, defect structures, or thermodynamic conditions. In addition, long-range electrostatics, polarization, and rare-event sampling remain challenging to capture consistently without explicit physical constraints. Consequently, ML predictions for graphene-based systems should be interpreted in conjunction with uncertainty awareness and, where possible, validated against atomistic simulations or experimental benchmarks.<sup>165</sup>

Additionally, Park *et al.* introduced GHP-MOF assemble, a generative AI framework for designing metal-organic frameworks (MOFs) for carbon capture, which combines molecular generative diffusion models with ML-based screening, MD, and GCMC simulations. Although focused on MOFs, the strategy demonstrates how generative AI can be adapted to graphene-based materials, particularly for adsorption, separation, and catalysis. Similar AI approaches could be applied to graphene oxide frameworks (GOFs) and covalent organic frameworks (COFs) for gas separation and pollutant removal. The CGCNN model, for example, could be retrained to predict graphene-adsorbate interactions, gas storage, and charge transport properties. Extending this methodology to graphene-MOF hybrids could yield high-surface-area materials for energy storage, supercapacitors, and electrochemical applications.<sup>166</sup>

## 7. Simulation of electrokinetic phenomena

Electrokinetic phenomena, such as ion transport, EDL formation, and electro-osmotic flows (EOFs), are fundamental to the operation of graphene-based membranes, nanopores, and electrochemical devices. Due to the multiscale nature of these processes, traditional MD or continuum approaches alone are often insufficient to capture the coupled electrostatic and hydrodynamic interactions across length and time scales. Recent advancements in DPD and its extensions have enabled more efficient and accurate mesoscale modeling of electrokinetic phenomena in complex systems, including graphene interfaces.

### 7.1. Charged DPD

Deng *et al.* introduced the charged dissipative particle dynamics framework (cDPD) as a mesoscale extension of classical DPD. In cDPD, each particle is assigned ionic concentration and



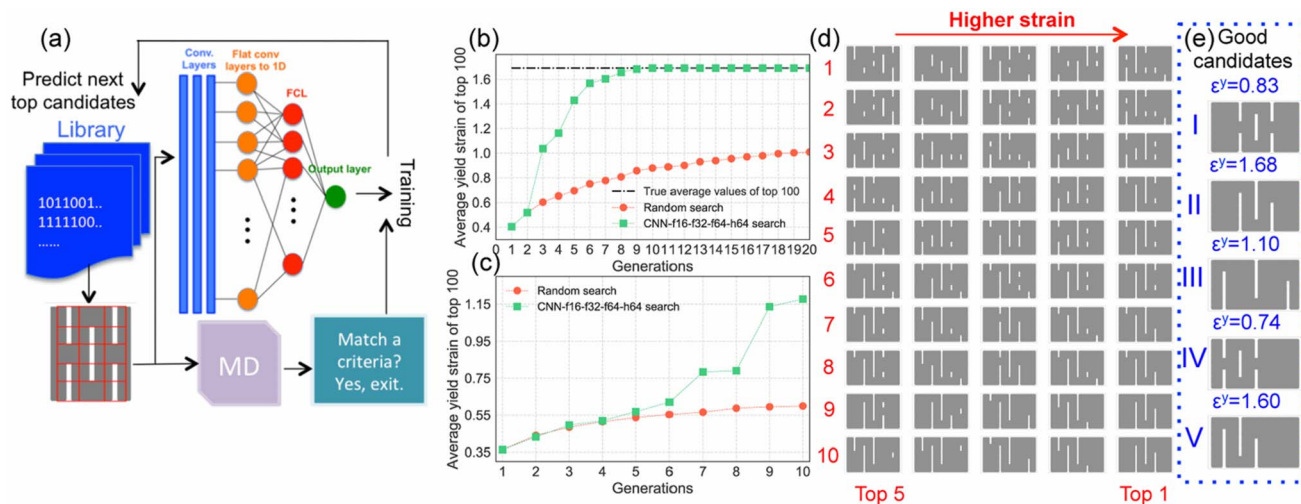


**Fig. 18** (a) Illustration of the neural network-based search algorithm for optimizing graphene kirigami patterns. Panels (b) and (c) plot the average yield strain of the top 100 configurations across generations for kirigami with  $3 \times 5$  and  $5 \times 5$  cut grids, respectively. Visualizations of the five best-performing  $5 \times 5$  configurations are shown for each generation, with the top three remaining unchanged after the ninth generation. (d) Shown are the top five kirigami performers with  $5 \times 5$  allowable cuts at each generation. After the ninth generation, the leading three configurations stabilize and no longer change. (e) Comparison between ML-optimized kirigami designs and conventional centered-cut patterns, demonstrating enhanced stretchability in the ML-generated configurations. Kirigami structures are not drawn to scale.<sup>162</sup> Reprinted figure with permission from Paul Z. Hanakata, Ekin D. Cubuk, David K. Campbell & Harold S. Park, *Phys. Rev. Lett.*, vol. 121, 255304 (2018). Copyright 2018 by the American Physical Society.

electrostatic potential, enabling the simultaneous solution of the stochastic Poisson–Nernst–Planck (PNP) and Navier–Stokes equations. This approach accurately models ion diffusion, electrostatic interactions, and thermal fluctuations using a fully Lagrangian scheme. The electrostatic potential is solved iteratively with a particle-based Poisson solver, eliminating the need for grid-based techniques. Enhanced boundary conditions enforce realistic hydrodynamic and electrostatic constraints at charged surfaces. Validation against Poisson–Boltzmann and mean-field solutions demonstrated cDPD’s accuracy for predicting EDL structure, EOF velocity profiles, and pressure-driven electrokinetic transport in microchannels. This method can be adapted to graphene membranes and nanopores by incorporating tunable surface charges and chemical functionalization, facilitating studies of ion sieving, desalination, and energy storage.<sup>167</sup>

## 7.2. Electrostatic DPD

González-Melchor *et al.*<sup>168</sup> and Gavrilo *et al.*<sup>169</sup> extended DPD by incorporating long-range electrostatic interactions through techniques such as Ewald summation and smoothly damped Coulomb forces. These modifications prevent unphysical charge collapse while preserving accuracy in systems with high charge density and non-uniform distributions. Electrostatic DPD has been validated by simulating polyelectrolyte chain collapse, ionic microphase separation, and electrolyte structuring, showing good agreement with MD simulations. For graphene-based materials, electrostatic DPD can be applied to model the dynamic behavior of ionic species near conductive surfaces, double-layer capacitance, and charge storage processes in supercapacitor electrodes. Such simulations offer insights into how surface charge distributions, defects, and

functional groups influence electro-osmotic transport and energy storage performance.

## 7.3. Many-body DPD and electronic transitions

Faramarzi and Mehdipour<sup>170</sup> applied many-body DPD to study the metal–nonmetal transition in fluid cesium, focusing on the role of atomic clustering, density fluctuations, and changes in electronic structure on conductivity. This methodology uses a grand canonical ensemble to track conductivity percolation by identifying connected atomic clusters, correlating structural dynamics with electronic transitions. While initially designed for liquid metals, this approach can be extended to graphene-based systems. Graphene’s electronic properties are highly sensitive to doping, strain, and external fields, which could be studied *via* many-body DPD to predict percolation thresholds, solvent-induced conductivity transitions, and charge transport pathways in composites. Recent parameterization strategies for many-body DPD at interfaces provide a solid foundation for adapting these models to simulate graphene/electrolyte interfaces.

## 8. Graphene ink

Printed electronics have emerged as a promising technology for fabricating low-cost, large-area, and flexible devices.<sup>171,172</sup> Conductive inks are central to this field, serving as the active material that forms electrical pathways and electrodes.<sup>173–180</sup> Their physical and chemical properties directly affect the performance, resolution, and stability of printed devices. Among conductive materials, graphene stands out due to its high electrical conductivity, chemical stability, and intrinsic flexibility.<sup>181–186</sup> Graphene-based inks provide a superior



alternative to conventional carbon-based inks, which often show limited conductivity in formulations suitable for inkjet printing.

To utilize graphene in inks, a large-area material that can be easily manipulated into complex device architectures is required. Among various production methods, solution-phase exfoliation is particularly attractive due to its low-cost precursors, scalability, low thermal budget, and compatibility with additive printing techniques.<sup>187–192</sup> While RGO has been used in inkjet printing for applications like thin-film transistors and sensors, its electrical properties are inferior to pristine graphene, making the latter more advantageous for high-performance printed electronics.<sup>193–197</sup>

Pristine graphene flakes can be obtained *via* ultrasonication in selected solvents<sup>198,199</sup> or with the use of additives such as planar surfactants and stabilizing polymers,<sup>200–202</sup> resulting in flakes smaller than 10  $\mu\text{m}^2$ . Small flakes are essential for stable inkjet printing, though they increase the number of flake-to-flake junctions, which can slightly raise film resistance. Moreover, traditional solvents and surfactants may leave residues even after extensive annealing, potentially disrupting the conductive network.<sup>187,203</sup> A holistic approach to graphene ink, therefore, involves exfoliation, ink formulation, printing, and final annealing, using environmentally friendly solvents like ethanol combined with stabilizing polymers such as ethyl cellulose, to achieve uniform, conductive, and flexible printed features suitable for next-generation electronic devices.

Printed electronics require inks that combine high conductivity, stability, and compatibility with flexible substrates. Among various preparation strategies, solution-phase exfoliation of graphene in environmentally friendly solvents such as ethanol, with stabilizing polymers like ethyl cellulose (EC), provides a scalable and effective route. Fig. 18 illustrates the preparation of graphene ink. First, graphene is exfoliated from graphite powder in an ethanol/EC mixture using probe ultrasonication to obtain thin graphene flakes. The resulting solution is then centrifuged to remove large graphite flakes, leaving only small, printable graphene flakes. Next, the graphene/EC flakes undergo salt-induced flocculation to form small aggregates, improving dispersion and reducing sedimentation. Finally, the graphene/EC powder is dispersed in an 85:15 cyclohexanone/terpineol mixture to produce a stable, inkjet-printable graphene ink shows the application of this ink onto a substrate. First, the flake morphology is examined with atomic force microscopy (AFM) to confirm the ink quality. The ink is then printed onto the substrate using an inkjet printer, forming small droplets. Finally, the printed patterns are annealed with intense pulsed light (IPL), which rapidly removes solvents, improves flake connectivity, and enhances conductivity.<sup>201,204</sup> In summary, Fig. 19 focuses on ink preparation, while Fig. 20 focuses on printing and post-processing to achieve uniform, conductive graphene patterns.<sup>204–207</sup>

In a recent study, the IPL annealing process was investigated as a rapid and substrate-compatible method for improving the electrical properties of inkjet-printed graphene films. As shown in Fig. 21, the sheet resistance of graphene films was evaluated as a function of light pulse energy on four different substrates,

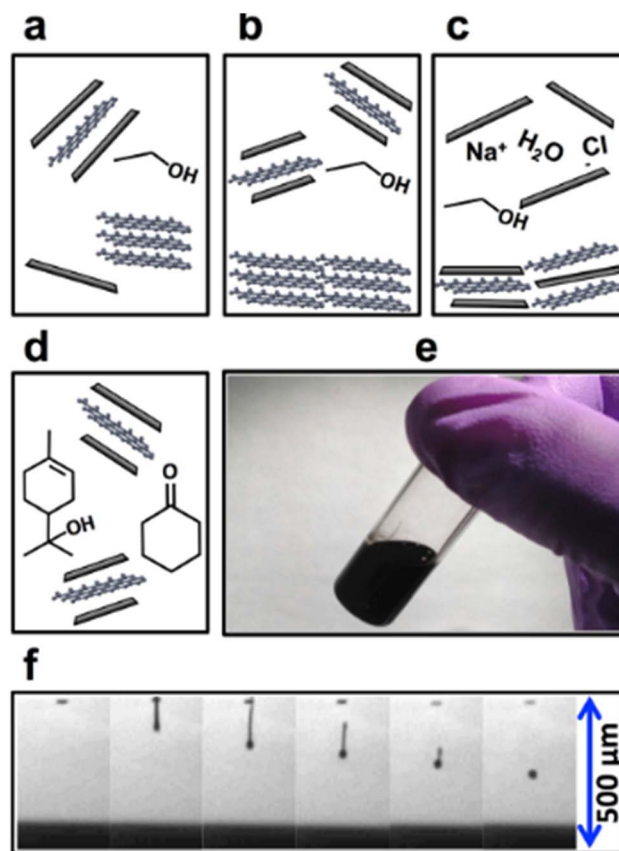


Fig. 19 Schematic illustration of the graphene ink preparation process. (a) Graphene flakes are exfoliated from graphite powder in an ethanol/ethyl cellulose (EC) mixture using probe ultrasonication. (b) The resulting graphene/EC dispersion is then centrifuged to remove large residual graphite flakes. (c) Salt-induced flocculation is applied to the graphene/EC to form small, stable aggregates. (d) The graphene/EC powder is subsequently dispersed in an 85:15 cyclohexanone/terpineol mixture to produce a stable ink suitable for inkjet printing. (e) Photograph of the prepared graphene ink in a vial. (f) Sequence of droplet formation during inkjet printing, showing spherical droplets forming after approximately 300  $\mu\text{m}$ . Adapted with permission from ref. 204. Copyright 2013 American Chemical Society.

including PET, PEN, polyimide (PI), and glass. The results indicate that, due to differences in the thermal properties of the substrates, the required pulse energy to achieve optimal conductivity varies. Substrates with lower thermal conductivity, such as PET and PEN, can produce highly conductive films even at low pulse energies, whereas thicker substrates like PI and glass require higher energy to achieve similar performance. Despite these differences, all substrates yielded graphene films with sheet resistance comparable to that obtained through conventional thermal annealing, demonstrating the versatility and efficiency of the IPL process.

Furthermore, examination of printed lines on various substrates, including PET, PEN, PI, glass, and HMDS-treated glass, revealed smooth, uniform patterns with well-defined edges and no coffee-ring effects, which confirms the excellent wetting and drying behavior of the graphene ink. Increasing the drop spacing was found to reduce the line width and improve



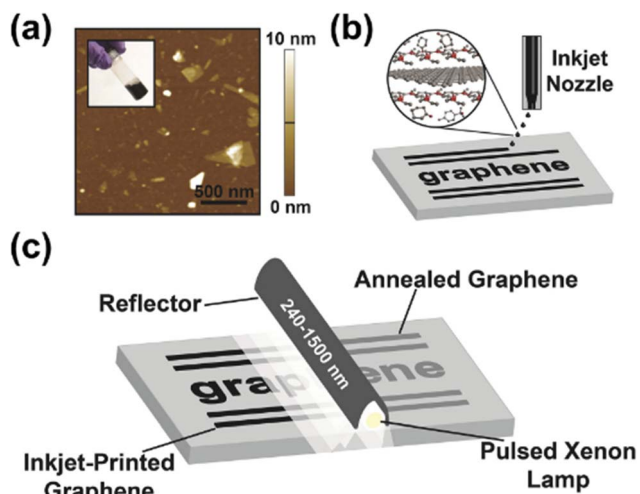


Fig. 20 Inkjet printing and intense pulsed light (IPL) annealing of graphene. (a) Atomic force microscopy (AFM) image of graphene flakes; the inset shows a vial of the graphene ink. (b) Schematic illustration of the inkjet printing process used to deposit graphene onto a substrate. (c) Schematic illustration of intense pulsed light (IPL) annealing applied to the printed graphene patterns to improve flake connectivity and conductivity. Adapted from ref. 207 with permission from Wiley, vol. 27, E. B. Secor, B. Y. Ahn, T. Z. Gao, J. A. Lewis & M. C. Hersam, "Rapid and versatile photonic annealing of graphene inks for flexible printed electronics", pp. 6683–6688, Copyright 2015 John Wiley and Sons.

the printing resolution, while surface treatment of the substrate with HMDS enabled the formation of fine lines with widths below 50  $\mu\text{m}$ . Overall, these findings clearly demonstrate that high-concentration graphene ink combined with IPL annealing provides a reliable approach for producing high-quality, conductive, and precise graphene patterns on a wide range of both flexible and rigid substrates.<sup>207</sup>

Recently, a method for preparing nitrocellulose-based graphene inks has been developed. In this approach, pristine graphite is exfoliated in a solution of nitrocellulose and acetone *via* shear mixing, and unexfoliated graphite flakes are removed by centrifugation, yielding a stable dispersion of few-layer graphene with a concentration of approximately 1  $\text{mg mL}^{-1}$ . AFM

characterization shows that the graphene platelets have an average thickness of  $\sim 2$  nm and lateral dimensions of  $\sim 200 \times 200$  nm, suitable for high-resolution printing. To simplify ink formulation, salt water is added to induce flocculation of the graphene/NC composite, which is then washed, dried, and obtained as a fine black powder that can be readily redispersed in suitable solvents. This approach allows precise control over ink properties such as concentration, surface tension, and drying kinetics, while enabling a wide range of viscosities suitable for various printing methods, including spray coating, blade coating, stencil, screen, gravure, and inkjet printing. For inkjet printing specifically, the graphene/NC powder is dispersed in a solvent mixture of ethyl lactate, octyl acetate, and ethylene glycol diacetate at a concentration of  $\sim 10$   $\text{mg mL}^{-1}$  to produce an ink with a shear viscosity of  $\sim 10$  mPa s, with low-volatility solvents included to prevent nozzle drying and to optimize wetting and drying behavior. Fig. 22 schematically illustrates this process and the ink characteristics; panel (a) shows the schematic preparation of the ink along with the nitrocellulose chemical structure and representative AFM images of graphene flakes, panel (b) presents the thickness distribution of the flakes with both number- and volume-weighted statistics, panel (c) displays the area distribution of the flakes, and panel (d) shows the shear viscosity of the graphene inks for different printing methods including blade coating, inkjet printing, and spray coating, emphasizing that the ink viscosity can be tuned over a wide range to suit various industrial printing and prototyping applications.<sup>208</sup>

Numerous simulation studies have been conducted on graphene inks to understand their behavior in inkjet printing applications. In a recent study, MD simulations were performed to investigate the behavior of graphene inks on plasma-modified polyimide (mPI) substrates. The main goal was to study interfacial adhesion, stability of the ink/substrate interface, and the effects of printing parameters such as inkjet velocity, temperature, and mechanical loading (pressure and deformation) at the atomic scale. Two types of inks were considered: GO and pristine graphene (PG), forming the mPI/GO and mPI/PG systems, respectively.

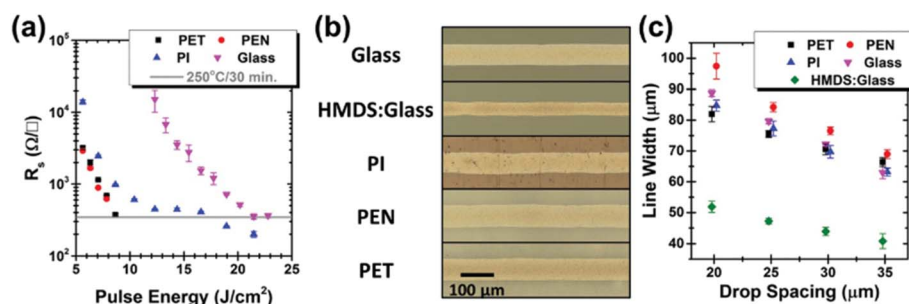


Fig. 21 Versatility of IPL annealing for printed graphene patterns. (a) Sheet resistance of graphene films as a function of annealing voltage on different substrates, including PET, PEN, polyimide (PI), and glass. (b) Optical microscopy images of printed lines on five different substrates with a droplet spacing of 35  $\mu\text{m}$ , showing uniform and well-defined patterns. (c) Resolution of inkjet-printed lines on the five substrates as a function of droplet spacing, demonstrating the effect of drop spacing on line width and printing precision. Adapted with permission from ref. 207 with permission from Wiley, vol. 27, E. B. Secor, B. Y. Ahn, T. Z. Gao, J. A. Lewis & M. C. Hersam, "Rapid and versatile photonic annealing of graphene inks for flexible printed electronics", pp. 6683–6688, Copyright 2015 John Wiley and Sons.



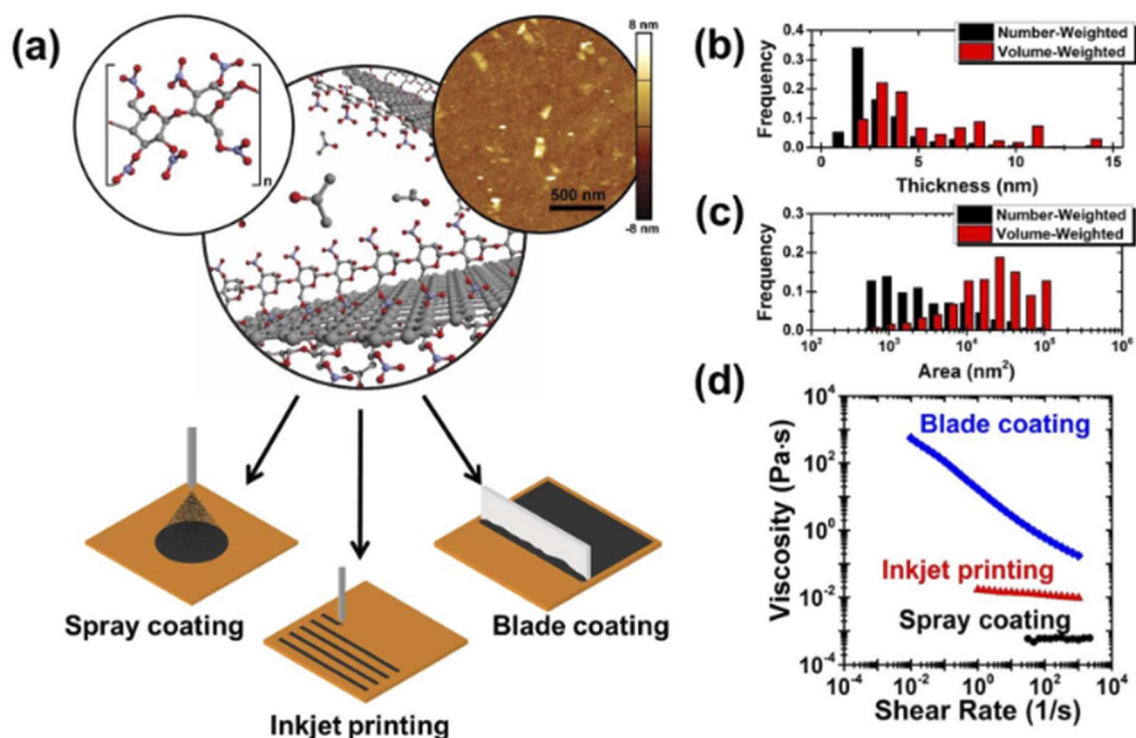


Fig. 22 Overview of the process and characterization of the graphene ink. (a) Schematic representation of the preparation and application of nitrocellulose-based graphene inks, showing the chemical structure of nitrocellulose (top left) and a representative AFM image of graphene flakes (top right). (b and c) Distributions of graphene flake thickness and lateral area, respectively, including both number-weighted and volume-weighted statistics obtained from AFM measurements (total number of flakes >600). (d) Shear viscosity of the graphene inks, optimized for different deposition techniques such as blade coating, inkjet printing, and spray coating Reprinted with permission from ref. 208, Copyright 2017 American Chemical Society.

Fig. 23 illustrates the simulation setup: the bottom part of the substrate is treated as rigid, and the ink is given an initial velocity toward the substrate (Fig. 23A). The results showed that the inkjet velocity affects two main aspects: the impact force of the ink on the substrate and the interfacial fluctuations at the ink/substrate interface, as reflected in the stress fluctuation amplitude (Fig. 23B) and the density profile of the ink near the interface (Fig. 23C and D). Generally, higher velocities lead to greater fluctuations in the interaction energy. However, in the mPI/GO system, higher inkjet velocities resulted in enhanced interfacial adhesion after approximately 100 ps, whereas no significant effect was observed for mPI/PG. These findings indicate that achieving uniform, stable, and conductive graphene patterns requires careful consideration of both impact force and interfacial fluctuations, providing valuable guidance for the development of graphene-based flexible electronics.<sup>209</sup> From an experimental perspective, these results highlight solvent selection, flake functionalization, and aggregation control as key parameters for achieving stable and printable graphene inks.

Recently, machine learning approaches have also been applied to graphene inks to predict and optimize their behavior in printing applications and final device performance. In a recent study, similar to strategies used for 3D-printed thermoplastics, a physics-informed machine learning (PIML) model was employed to predict the properties of different graphene

inks.<sup>210</sup> Initially, MD simulations were performed to investigate the interfacial adhesion and stability of the ink/substrate interface under various printing conditions, including inkjet velocity, temperature, and mechanical loading. Subsequently, a multilayer perceptron (MLP) model was used to predict the characteristics of different graphene inks. By reducing the dimensionality of experimental data and incorporating physics-informed descriptors, the model achieved highly accurate predictions and established correlations between ink composition and performance. These results demonstrate that combining MD simulations with machine learning provides an effective strategy for optimizing graphene inks and designing flexible, conductive printed patterns.

## 9. Comparison of simulation approaches for graphene

In the previous sections of this article, we reviewed the details of atomistic simulations of graphene, coarse-grained (CG) methods, and machine learning (ML) applications, providing examples from studies on structural, mechanical, and defective graphene behavior. We also discussed how these approaches can be used to predict material properties and investigate interfacial interactions. Table 3 provides a comprehensive comparison of the main simulation approaches for graphene, including atomistic simulations, Coarse-Grained (CG) methods,



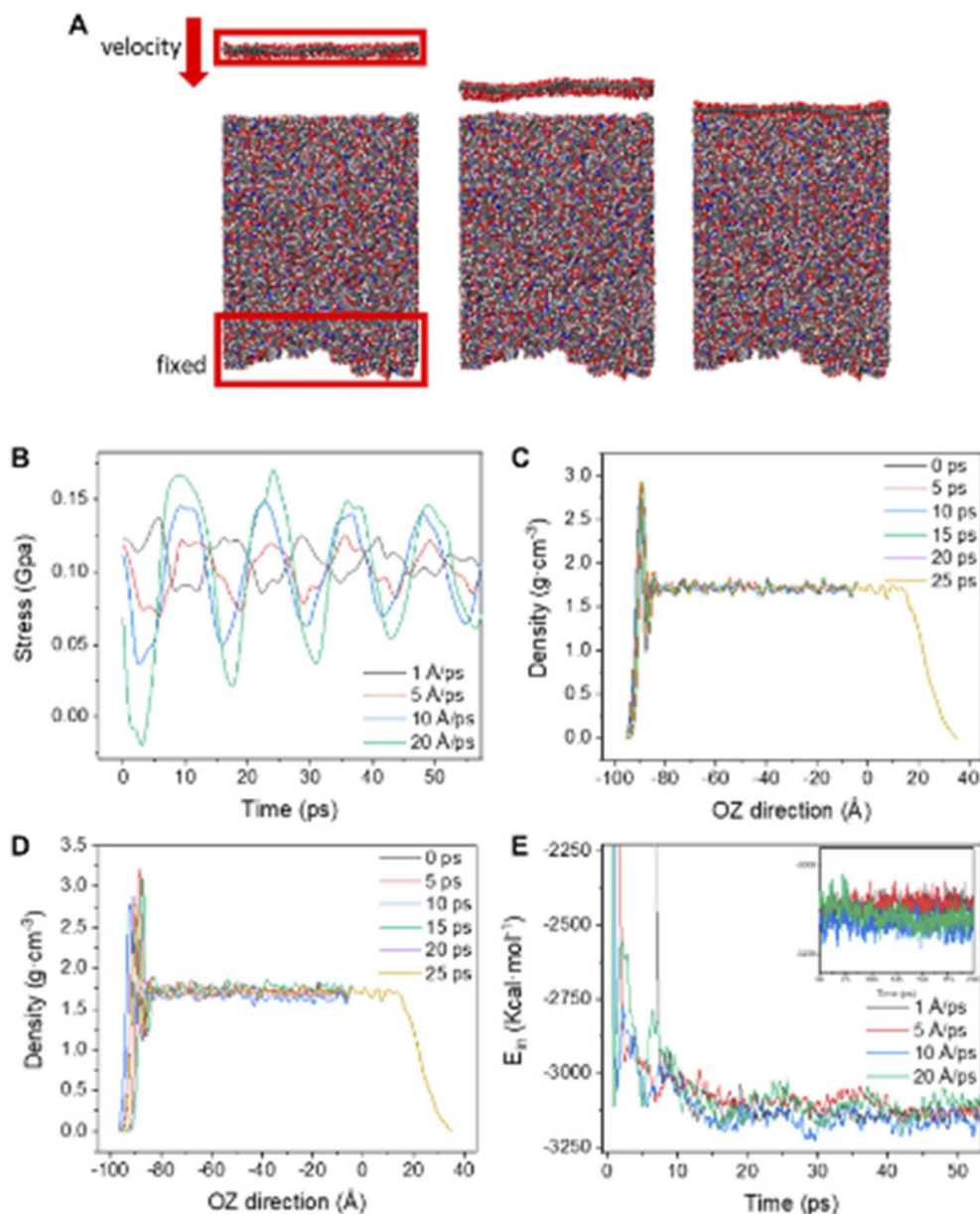


Fig. 23 (A) Scheme of shooting GO onto mPI; (B) stress of mPI/GO upon hitting; density profiles of mPI/GO system under (C) 1 Å ps<sup>-1</sup>, (D) 10 Å ps<sup>-1</sup>; (E)  $E_{in}$  change of mPI/GO system under different inkjet velocities upon hitting; inset: magnified  $E_{in}$  change from 50 to 200 ps. Adapted from "Adapted from ref. 209, licensed under CC BY 4.0".

and Machine Learning (ML) techniques. The table highlights the spatial and temporal scales, primary applications, strengths, and limitations of each method. Atomistic simulations, operating at atomic resolution (Å) and femtosecond timescales (fs), allow detailed investigation of graphene's structural, mechanical, electronic, and thermal properties. These simulations can capture interfacial interactions, adsorption of molecules, and behaviors of defective graphene, providing directly interpretable physical quantities. However, their main limitation lies in high computational cost, restricting studies to small systems and short simulation durations, which prevents exploration of large-scale or long-term phenomena.<sup>211</sup>

Coarse-Grained approaches reduce atomic detail by grouping atoms into effective particles, allowing simulations over larger spatial (nm–μm) and temporal (μs–ms) scales. These methods efficiently study large-scale dynamics, self-assembly, realistic mechanical deformation, and fluid interactions. They can include hydrodynamic effects and bridge molecular and continuum scales. The trade-off is the loss of atomic-level detail and inability to capture quantum or electronic effects.<sup>212</sup> Machine learning techniques leverage atomic or experimental data to rapidly predict material properties, fit potential energy surfaces, and discover new materials. They are fast, transferable, and enable multi-scale integration, extending predictive capability beyond traditional simulation datasets. Their



Table 4 Comparison between atomistic simulations, coarse-grained (CG), and machine learning (ML) approaches

Method	Scale & resolution	Main applications	Advantages	Limitations
Atomistic	Atomic scale (Å, fs)	Structural, mechanical, electronic, and thermal properties of pristine and defective graphene; interfacial interactions; and adsorption studies	High accuracy, captures bond formation/breaking, directly interpretable physical quantities	Computationally expensive, limited to small systems and short timescales
Coarse-grained (CG)	Mesoscale (nm–μm, μs–ms)	Large-scale dynamics of graphene-based composites, membranes, and fluids; self-assembly; mechanical deformation under realistic conditions	Efficient for large systems, includes hydrodynamic effects, bridges molecular and continuum scales	Lacks atomic detail. Parameterization can be system dependent. Not suitable for quantum or electronic effects
Machine learning (ML)	Cross-scale (trained from atomic or experimental data)	Property prediction, potential energy surface fitting, materials discovery, optimization of synthesis conditions	Very fast once trained, transferable, enables multi-scale integration and prediction beyond simulation data	Requires large, high-quality datasets, limited interpretability, may fail outside the training domain

limitations include the need for high-quality training data and reduced reliability outside the training domain 213.

Table 4 summarizes the major challenges in computational modeling of graphene and outlines practical strategies to address them. One of the primary limitations arises from the restricted scale of atomistic simulations. Although MD offers atomic-level precision, it is computationally expensive and limited to small systems. To overcome this, multi-scale modeling using CG and ML approaches has been proposed, enabling the efficient exploration of larger and longer systems. The second challenge involves uncontrolled structural defects, which are often introduced during non-ideal graphene synthesis. This issue can be mitigated by simulating the growth process in conjunction with ML-assisted optimization, thereby improving defect prediction and control.

For multi-functional property prediction, bridging the gap between atomic and macroscopic scales remains a major difficulty. Integrating multi-scale and modular simulation frameworks (MD–CG–ML) provides a coherent link between structure and function, enhancing the predictive capability of simulations. While CG simulations enable large-scale studies, they inherently lose atomic detail. Therefore, hybrid MD–CG methods are necessary to retain atomic accuracy while

maintaining computational efficiency. Finally, ML models are often limited by their training datasets, which can reduce reliability outside the training domain. Expanding high-quality datasets and coupling ML with physical simulations are essential for improving robustness and generalization. Overall, Table 4 highlights that no single simulation technique is sufficient to capture the full behavior of graphene. Instead, an intelligent integration of MD, CG, and ML methods provides the balance between atomic accuracy, scalability, and predictive power, a crucial step toward designing next-generation graphene-based materials (Table 5).<sup>214–218</sup>

The correlation between the properties and performance of graphene shown in Fig. 24 is derived from experimental and computational data reported in previous studies,<sup>7,13,181,184,219–224</sup> integrating mechanical,<sup>7,219</sup> electrical,<sup>181,220</sup> and thermal<sup>13,223</sup> characteristics of graphene for various applications. This figure presents a radar chart that visually and quantitatively illustrates the relationship between the intrinsic properties of graphene and its suitability for different applications. The axes of the chart represent key properties, including fracture strain, fracture strength, Young's modulus, electrical conductivity, and thermal conductivity. Each colored line corresponds to a specific application of graphene such as flexible electronics,

Table 5 Key challenges in computational modeling of graphene and corresponding strategies proposed to overcome them using different simulation methodologies

Challenge	Reason	Proposed solution (and related method)
Scale limitation	MD is computationally expensive and limited to a few thousand atoms	Employ multi-scale simulations using CG or ML approaches
Uncontrolled defects	Non-ideal synthesis of graphene leads to structural defects	Simulate growth processes combined with ML-assisted optimization
Multi-functional property prediction	Difficult to bridge atomic and macroscopic scales	Integrate multi-scale and modular simulation frameworks (MD–CG–ML)
Loss of atomic detail	CG simulations sacrifice atomic resolution	Apply hybrid MD–CG approaches to retain atomistic accuracy
Limited training domain	ML models may fail outside the training dataset	Expand high-quality datasets and couple ML with physical simulations



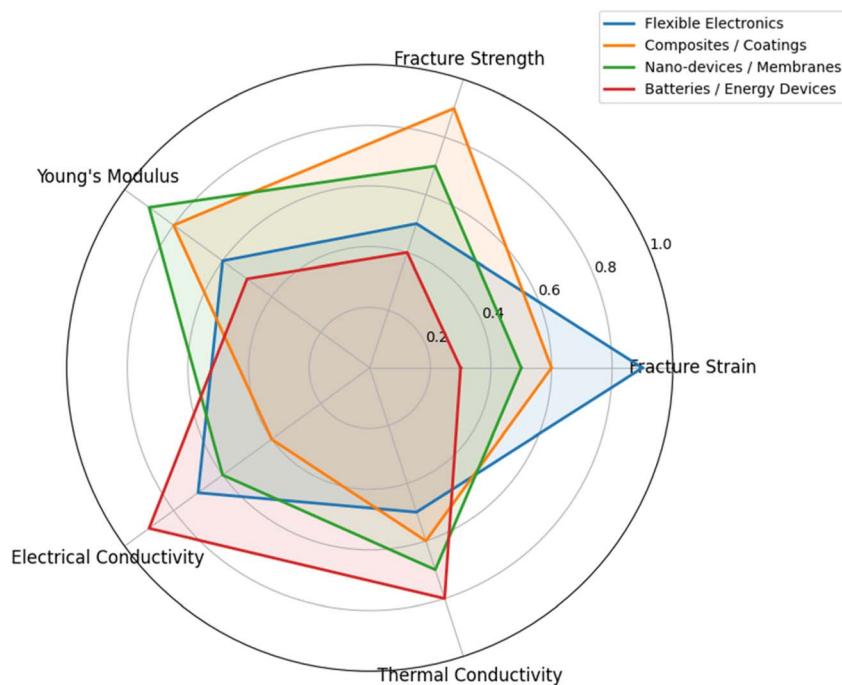


**Fig. 24** Radar chart showing the suitability of graphene properties for different applications. The axes represent key properties including fracture strain, fracture strength, Young's modulus, electrical conductivity, and thermal conductivity. Each colored line corresponds to a specific application flexible electronics, composites/coatings, nano-devices/membranes, and batteries/energy devices and the values (0–1) indicate how critical each property is for that application. The chart illustrates how graphene's mechanical, electrical, and thermal characteristics collectively influence its performance across applications and provides a quantitative guide for material design and optimization.

composites and coatings, nano-devices and membranes, and batteries or energy storage systems and the values from 0 to 1 indicate the relative importance of each property for that particular application. A high fracture strain allows graphene to stretch without breaking, which is essential for flexible electronics.

A high fracture strength enables graphene to withstand large mechanical loads, improving the durability of composites and coatings. A higher Young's modulus contributes to stiffness and mechanical stability, enhancing the structural integrity of composites and the stability of nano-devices. High electrical conductivity ensures efficient charge transport, which is vital for batteries, supercapacitors, and electronic devices, while also supporting reliable signal transmission in flexible electronics. Similarly, high thermal conductivity allows for effective heat dissipation, preventing damage in nano-devices, high-power electronics, and energy systems, and improving thermal management in advanced composites. Overall, this radar chart demonstrates how the combination of graphene's mechanical, electrical, and thermal properties determines its performance across various applications.

## 10. Conclusion and outlook

This review highlights the remarkable progress in multiscale modeling of graphene and its derivatives, encompassing atomistic molecular dynamics, coarse-grained simulations, and emerging machine learning approaches. By integrating insights from mechanical, thermal, and mass transport studies, as well

as defect engineering and chemical functionalization, we have demonstrated how computational methods bridge atomic-scale phenomena with device-scale performance. The unique strength of multiscale frameworks lies in their ability to capture critical structure–property relationships that guide the rational design of graphene-based systems for advanced applications in electronics, energy storage, filtration, and flexible devices. Despite these advances, challenges remain, including the need for improved force field accuracy, seamless coupling of models across scales, and rigorous experimental validation. Machine learning-driven force fields and AI-accelerated simulations offer promising solutions to these challenges, enabling rapid and predictive exploration of vast structural and chemical spaces. Future research should focus on combining high-throughput simulations, data-driven design, and experimental feedback loops to develop scalable, reliable, and application-specific graphene materials. In essence, multiscale modeling is evolving from a supporting tool to a predictive engine for innovation in graphene science, paving the way for next-generation functional materials and technologies.

Graphene research has followed a remarkable trajectory, evolving from theoretical predictions in the mid-20th century to groundbreaking experimental achievements in the early 2000s, and now entering the era of predictive multiscale modeling. Molecular simulations have become indispensable tools for uncovering the structural, mechanical, thermal, and interfacial behaviors of graphene and its derivatives. Despite significant advances, numerous scientific and engineering challenges remain that limit the full exploitation of this extraordinary



material. Future studies should emphasize the seamless integration of theory and experiment. Multiscale models must be closely aligned with experimental observations to enable accurate predictions of both material properties and fabrication processes. There is a critical need to develop quantitative frameworks to capture the effects of strain, curvature, and symmetry breaking on electronic properties, such as band structure, conductivity, and charge transport, which are particularly relevant for the design of flexible electronics, sensors, and novel nanoscale devices.

Simulation-guided processing and self-assembly also represent an emerging frontier. While the mechanics and dispersion of graphene have been extensively studied, the use of simulations to guide practical processes—such as solvent selection, ink formulation, flow-induced self-assembly, and large-scale functionalization—remains underdeveloped. By predicting processing–structure–property relationships, future modeling efforts can accelerate the translation of graphene research from the laboratory to industrial applications, minimizing trial-and-error experimentation. Defect engineering offers additional opportunities. While defects are often considered detrimental, their controlled introduction can enhance selective transport, catalysis, and separation performance. Advanced simulations should quantify the effects of defect patterns on material properties across multiple scales, enabling the rational design of membranes and nanostructures with tunable mechanical strength, selectivity, and functionality.

The integration of machine learning with multiscale modeling promises to revolutionize the field. Hybrid workflows that combine the chemical fidelity of atomistic simulations with the scalability of CG and DPD models can accelerate the design of nanocomposites, inks, and membranes, providing more accurate predictions of material behavior and process outcomes. Furthermore, shape-aware coarse-graining, using ellipsoidal, rod-like, or patchy particles, is necessary to capture graphene's anisotropic and planar nature more realistically, improving predictions of directional interactions and self-assembly behavior. The long-term vision involves creating a “Graphene Materials Studio”, an integrated digital platform capable of predicting not only the final properties of graphene-based materials but also optimal fabrication protocols, defect management, and morphological outcomes. Such a platform would allow researchers and engineers to digitally prototype materials, bridging the gap between design, synthesis, and performance, and enabling rapid innovation with minimal trial and error.

In summary, achieving predictive design and scalable applications of graphene requires an intelligent combination of multiscale modeling, machine learning, and the integration of theory with experiment. By leveraging these strategies, the full potential of graphene can be unlocked, advancing both fundamental understanding and practical deployment of next-generation materials.

## Conflicts of interest

There are no conflicts of interest to declare.

## Abbreviations

2D	Two-dimensional
ANN	Artificial neural network
CG	Coarse-grained
CGCNN	Crystal graph convolutional neural network
CGMD	Coarse-grained molecular dynamics
CGNS	Coarse-grained graphene nanosheet
CNN	Convolutional neural network
CNT	Carbon nanotube
COF	Covalent organic framework
cDPD	Charged dissipative particle dynamics
CSDS	Coarse-grained sodium dodecyl sulfate
DFT	Density functional theory
DPD	Dissipative particle dynamics
EC	Ethyl cellulose
EDL	Electrical double layer
EOF	Electro-osmotic flow
FEM	Finite element method
FGN	Functionalized graphene nanosheet
GO	Graphene oxide
GNN	Graph neural network
h-BN	Hexagonal boron nitride
IBI	Iterative boltzmann inversion
kMC	Kinetic monte carlo
LIE	Linear interaction energy
LJ	Lennard-Jones
LSTM	Long short-term memory (neural network)
MD	Molecular dynamics
MDFP	Molecular dynamics fingerprint
ML	Machine learning
MLFF	Machine-learned force field
MLG	Multilayer graphene
MLIP	Machine-learned interatomic potential
MOF	Metal–organic framework
NEMD	Non-equilibrium molecular dynamics
NNP	Neural network potential
NPG	Nanoporous graphene
PEO	Polyethylene oxide
PMMA	Poly(methyl methacrylate)
PNP	Poisson–Nernst–Planck
PVDF	Polyvinylidene fluoride
PVP	Polyvinylpyrrolidone
RF	Random forest
rGO	Reduced graphene oxide
SAXS	Small-angle X-ray scattering
SC	Single-crystalline
SDS	Sodium dodecyl sulfate
SE(3)	Special euclidean group (3D transformations)
STW	Stone–Thrower–Wales
SW	Stone–Wales
SVM	Support vector machine

## Data availability

This review article does not contain any new experimental, computational, or simulation data. All results, figures, and



datasets referenced in the manuscript are derived from previously published studies, which are cited in full in the References section. No new primary data was created for this work.

## Acknowledgements

We acknowledge the financial support provided by the National Science Foundation (NSF) through the Future Manufacturing MADE-PUBLIC program (Grant No. 2037026), which made this research possible.

## References

- 1 S. Bhattacharyya, *Carbon Superstructures: from Quantum Transport to Quantum Computation*, CRC Press, 2024.
- 2 B. I. Kharisov and O. V. Kharissova, *Carbon Allotropes: Metal-Complex Chemistry, Properties and Applications*, Springer, 2019.
- 3 X. Tang, Unveiling the Properties, Structure, and Preparation of Monoelemental Main Group Xenon for Enhanced Nonlinear Optics Applications, *J. Mater. Chem. C*, 2025, **13**(24), 12098–12126.
- 4 A. Kausar, *Graphene to Polymer/Graphene Nanocomposites: Emerging Research and Opportunities*, 2021.
- 5 A. H. Castro Neto, *et al.*, The electronic properties of graphene, *Rev. Mod. Phys.*, 2009, **81**(1), 109–162.
- 6 J. Zhang, *et al.*, A comprehensive review on the molecular dynamics simulation of the novel thermal properties of graphene, *RSC Adv.*, 2015, **5**(109), 89415–89426.
- 7 C. Lee, *et al.*, Measurement of the elastic properties and intrinsic strength of monolayer graphene, *Science*, 2008, **321**(5887), 385–388.
- 8 A. Ballestar, P. Esquinazi, J. Barzola-Quiquia, S. Dusari, F. Bern, R. R. da Silva and I. V. Kolesovich, Possible superconductivity in multi-layer graphene by application of a gate voltage, *Carbon*, 2014, **72**, 312–320.
- 9 Y. P. Bliokh, V. Freilikher and F. Nori, Ballistic charge transport in graphene and light propagation in periodic dielectric structures with metamaterials: A comparative study, *Phys. Rev. B: Condens. Matter Mater. Phys.*, 2013, **87**(24), 245134.
- 10 V. Ilyasov, *et al.*, Semiconductor–halfmetal–metal transition and magnetism of bilayer graphene nanoribbons/hexagonal boron nitride heterostructure, *Solid State Commun.*, 2014, **199**, 1–10.
- 11 Q.-Y. Li, *et al.*, Measurement of specific heat and thermal conductivity of supported and suspended graphene by a comprehensive Raman optothermal method, *Nanoscale*, 2017, **9**(30), 10784–10793.
- 12 A. A. Balandin, *et al.*, Superior thermal conductivity of single-layer graphene, *Nano Lett.*, 2008, **8**(3), 902–907.
- 13 A. A. Balandin, Thermal properties of graphene and nanostructured carbon materials, *Nat. Mater.*, 2011, **10**(8), 569–581.
- 14 B. C. Brodie, XIII. On the atomic weight of graphite, *Phil. Trans. Roy. Soc. Lond.*, 1859, (149), 249–259.
- 15 W. S. Hummers Jr and R. E. Offeman, Preparation of graphitic oxide, *J. Am. Chem. Soc.*, 1958, **80**(6), 1339.
- 16 A. Van Bommel, J. Crombeen and A. Van Tooren, LEED and Auger electron observations of the SiC (0001) surface, *Surf. Sci.*, 1975, **48**(2), 463–472.
- 17 K. S. Novoselov, *et al.*, Electric field effect in atomically thin carbon films, *Science*, 2004, **306**(5696), 666–669.
- 18 F. Bonaccorso, *et al.*, Production and processing of graphene and 2d crystals, *Mater. Today*, 2012, **15**(12), 564–589.
- 19 Y. Hancock, The 2010 Nobel Prize in physics—ground-breaking experiments on graphene, *J. Phys. D: Appl. Phys.*, 2011, **44**(47), 473001.
- 20 S. N. Alam, N. Sharma and L. Kumar, Synthesis of graphene oxide (GO) by modified hummers method and its thermal reduction to obtain reduced graphene oxide (rGO), *Graphene*, 2017, **6**(01), 1.
- 21 S. Ray, *Applications of Graphene and Graphene-Oxide Based Nanomaterials*, William Andrew, 2015.
- 22 N. Sharma, *et al.*, Synthesis and characterization of graphene oxide (GO) and reduced graphene oxide (rGO) for gas sensing application, in *Macromolecular Symposia*, Wiley Online Library, 2017.
- 23 Z. Bo, *et al.*, Green preparation of reduced graphene oxide for sensing and energy storage applications, *Sci. Rep.*, 2014, **4**(1), 4684.
- 24 P. Zhang, *et al.*, Recent advances in effective reduction of graphene oxide for highly improved performance toward electrochemical energy storage, *Energy Environ. Mater.*, 2018, **1**(1), 5–12.
- 25 T. S. Sreeprasad, *et al.*, Reduced graphene oxide–metal/metal oxide composites: facile synthesis and application in water purification, *J. Hazard Mater.*, 2011, **186**(1), 921–931.
- 26 W. Jung, *et al.*, An efficient reduced graphene-oxide filter for PM 2.5 removal, *J. Mater. Chem. A*, 2018, **6**(35), 16975–16982.
- 27 H. Yamaguchi, *et al.*, Reduced graphene oxide thin films as ultrabarrriers for organic electronics, *Adv. Energy Mater.*, 2014, **4**(4), 1300986.
- 28 C. Chung, *et al.*, Biomedical applications of graphene and graphene oxide, *Accounts Chem. Res.*, 2013, **46**(10), 2211–2224.
- 29 L. Feng, L. Wu and X. Qu, New horizons for diagnostics and therapeutic applications of graphene and graphene oxide, *Adv. Mater.*, 2013, **25**(2), 168–186.
- 30 A. Gholampour, *et al.*, From graphene oxide to reduced graphene oxide: impact on the physiochemical and mechanical properties of graphene–cement composites, *ACS Appl. Mater. Interfaces*, 2017, **9**(49), 43275–43286.
- 31 A. Page, *et al.*, Insights into carbon nanotube and graphene formation mechanisms from molecular simulations: a review, *Rep. Prog. Phys.*, 2015, **78**(3), 036501.
- 32 J. Tersoff, New empirical approach for the structure and energy of covalent systems, *Phys. Rev. B: Condens. Matter Mater. Phys.*, 1988, **37**(12), 6991.



- 33 A. C. Van Duin, *et al.*, ReaxFF: a reactive force field for hydrocarbons, *J. Phys. Chem. A*, 2001, **105**(41), 9396–9409.
- 34 D. Kauzlaric, *et al.*, Bottom-up coarse-graining of a simple graphene model: The blob picture, *J. Chem. Phys.*, 2011, **134**(6), 064106.
- 35 P. Rowe, *et al.*, Development of a machine learning potential for graphene, *Phys. Rev. B*, 2018, **97**(5), 054303.
- 36 L. Safina, *et al.*, Simulation of metal-graphene composites by molecular dynamics: a review, *Lett. Mater.*, 2020, **10**(3), 351–360.
- 37 S. H. Min, C. Lee and J. Jang, Dissipative particle dynamics modeling of a graphene nanosheet and its self-assembly with surfactant molecules, *Soft Matter*, 2012, **8**(33), 8735–8742.
- 38 L. Ruiz, *et al.*, A coarse-grained model for the mechanical behavior of multi-layer graphene, *Carbon*, 2015, **82**, 103–115.
- 39 S. Liu, *et al.*, A multilayer coarse-grained molecular dynamics model for mechanical analysis of mesoscale graphene structures, *Carbon*, 2021, **178**, 528–539.
- 40 J.-J. Shang, Q.-S. Yang and X. Liu, New coarse-grained model and its implementation in simulations of graphene assemblies, *J. Chem. Theor. Comput.*, 2017, **13**(8), 3706–3714.
- 41 K. T. Butler, *et al.*, Machine learning for molecular and materials science, *Nature*, 2018, **559**(7715), 547–555.
- 42 V. L. Deringer, *et al.*, Origins of structural and electronic transitions in disordered silicon, *Nature*, 2021, **589**(7840), 59–64.
- 43 H.-J. Kim, K.-J. Seo and D.-E. Kim, Investigation of mechanical behavior of single- and multi-layer graphene by using molecular dynamics simulation, *Int. J. Precis. Eng. Manuf.*, 2016, **17**, 1693–1701.
- 44 J. Zang, *et al.*, Multifunctionality and control of the crumpling and unfolding of large-area graphene, *Nat. Mater.*, 2013, **12**(4), 321–325.
- 45 S. Cranford and M. J. Buehler, Twisted and coiled ultralong multilayer graphene ribbons, *Model. Simulat. Mater. Sci. Eng.*, 2011, **19**(5), 054003.
- 46 M. Chen, *et al.*, Effects of grain size, temperature and strain rate on the mechanical properties of polycrystalline graphene—A molecular dynamics study, *Carbon*, 2015, **85**, 135–146.
- 47 Q. Pei, Y. Zhang and V. Shenoy, A molecular dynamics study of the mechanical properties of hydrogen functionalized graphene, *Carbon*, 2010, **48**(3), 898–904.
- 48 Y. Li, *et al.*, Mechanical properties of hydrogen functionalized graphene allotropes, *Comput. Mater. Sci.*, 2014, **83**, 212–216.
- 49 Q. Lu, W. Gao and R. Huang, Atomistic simulation and continuum modeling of graphene nanoribbons under uniaxial tension, *Model. Simulat. Mater. Sci. Eng.*, 2011, **19**(5), 054006.
- 50 M. Jahanshahi, M. Vokhshoori and A. Khoei, A coarse-graining approach for modeling nonlinear mechanical behavior of FCC nano-crystals, *Comput. Mater. Sci.*, 2020, **172**, 109357.
- 51 Q. Bao, *et al.*, Effects of graphene thickness and length distribution on the mechanical properties of graphene networks: A coarse-grained molecular dynamics simulation, *Appl. Surf. Sci.*, 2021, **570**, 151023.
- 52 Y. Shen and H. Wu, Interlayer shear effect on multilayer graphene subjected to bending, *Appl. Phys. Lett.*, 2012, **100**(10), 109109.
- 53 G. Wang, *et al.*, Measuring interlayer shear stress in bilayer graphene, *Phys. Rev. Lett.*, 2017, **119**(3), 036101.
- 54 O. Liba, *et al.*, A dissipative particle dynamics model of carbon nanotubes, *Mol. Simul.*, 2008, **34**(8), 737–748.
- 55 P. Zhang, *et al.*, Fracture toughness of graphene, *Nat. Commun.*, 2014, **5**(1), 3782.
- 56 M. Dewapriya and S. Meguid, Atomistic modeling of out-of-plane deformation of a propagating Griffith crack in graphene, *Acta Mech.*, 2017, **228**, 3063–3075.
- 57 Y. Wei, *et al.*, The nature of strength enhancement and weakening by pentagon–heptagon defects in graphene, *Nat. Mater.*, 2012, **11**(9), 759–763.
- 58 A. K. Singh and R. G. Hennig, Scaling relation for thermal ripples in single and multilayer graphene, *Phys. Rev. B: Condens. Matter Mater. Phys.*, 2013, **87**(9), 094112.
- 59 A. Mauri, D. Soriano and M. I. Katsnelson, Thermal ripples in bilayer graphene, *Phys. Rev. B*, 2020, **102**(16), 165421.
- 60 B. I. Yakobson, C. Brabec and J. Bernholc, Nanomechanics of carbon tubes: instabilities beyond linear response, *Phys. Rev. Lett.*, 1996, **76**(14), 2511.
- 61 Q. Lu and B. Bhattacharya, Effect of randomly occurring Stone–Wales defects on mechanical properties of carbon nanotubes using atomistic simulation, *Nanotechnology*, 2005, **16**(4), 555.
- 62 J.-P. Salvetat, *et al.*, Mechanical properties of carbon nanotubes, *Appl. Phys. A: Mater. Sci. Process.*, 1999, **69**(3), 255–260.
- 63 B. Arash, H. S. Park and T. Rabczuk, Mechanical properties of carbon nanotube reinforced polymer nanocomposites: A coarse-grained model, *Composites, Part B*, 2015, **80**, 92–100.
- 64 J. Chen, *et al.*, A review of the interfacial characteristics of polymer nanocomposites containing carbon nanotubes, *RSC Adv.*, 2018, **8**(49), 28048–28085.
- 65 F. Lin, *et al.*, Morphological and mechanical properties of graphene-reinforced PMMA nanocomposites using a multiscale analysis, *Comput. Mater. Sci.*, 2018, **150**, 107–120.
- 66 H. Zhao, K. Min and N. R. Aluru, Size and chirality dependent elastic properties of graphene nanoribbons under uniaxial tension, *Nano Lett.*, 2009, **9**(8), 3012–3015.
- 67 R. Ansari, S. Ajori and B. Motevalli, Mechanical properties of defective single-layered graphene sheets via molecular dynamics simulation, *Superlattices Microstruct.*, 2012, **51**(2), 274–289.
- 68 Z. Ni, *et al.*, Anisotropic mechanical properties of graphene sheets from molecular dynamics, *Phys. B*, 2010, **405**(5), 1301–1306.
- 69 Z. Zhang, *et al.*, Accelerated discoveries of mechanical properties of graphene using machine learning and high-throughput computation, *Carbon*, 2019, **148**, 115–123.



- 70 X. Huang, *et al.*, Graphene-based electrodes, *Adv. Mater.*, 2012, **24**(45), 5979–6004.
- 71 K. E. Karim, *et al.*, Estimating water transport in carbon nanotubes: A critical review and inclusion of scale effects, *Phys. Chem. Chem. Phys.*, 2024, **26**(28), 19069–19082.
- 72 K. Falk, *et al.*, Molecular origin of fast water transport in carbon nanotube membranes: superlubricity versus curvature dependent friction, *Nano Lett.*, 2010, **10**(10), 4067–4073.
- 73 E. Secchi, *et al.*, Massive radius-dependent flow slippage in carbon nanotubes, *Nature*, 2016, **537**(7619), 210–213.
- 74 S. Ghosh, *et al.*, Extremely high thermal conductivity of graphene: Prospects for thermal management applications in nanoelectronic circuits, *Appl. Phys. Lett.*, 2008, **92**(15), 101909.
- 75 L. A. Jauregui, *et al.*, Thermal transport in graphene nanostructures: Experiments and simulations, *ECS Trans.*, 2010, **28**(5), 73.
- 76 W. Cai, *et al.*, Thermal transport in suspended and supported monolayer graphene grown by chemical vapor deposition, *Nano Lett.*, 2010, **10**(5), 1645–1651.
- 77 J. Li and J. Zhang, Thermal transport properties of defective graphene/graphyne van der Waals heterostructures elucidated via molecular dynamics and machine learning, *Nanoscale*, 2024, **16**(38), 17992–18004.
- 78 J. Tersoff, Modeling solid-state chemistry: Interatomic potentials for multicomponent systems, *Phys. Rev. B: Condens. Matter Mater. Phys.*, 1989, **39**(8), 5566.
- 79 S. J. Stuart, A. B. Tutein and J. A. Harrison, A reactive potential for hydrocarbons with intermolecular interactions, *J. Chem. Phys.*, 2000, **112**(14), 6472–6486.
- 80 D. W. Brenner, *et al.*, A second-generation reactive empirical bondorder (REBO) potential energy expression for hydrocarbons, *J. Phys.: Condens. Matter*, 2002, **14**(4), 783.
- 81 L. Lindsay and D. Broido, Optimized Tersoff and Brenner empirical potential parameters for lattice dynamics and phonon thermal transport in carbon nanotubes and graphene, *Phys. Rev. B: Condens. Matter Mater. Phys.*, 2010, **81**(20), 205441.
- 82 Z. Wei, *et al.*, In-plane lattice thermal conductivities of multilayer graphene films, *Carbon*, 2011, **49**(8), 2653–2658.
- 83 Y. Hong, *et al.*, Phonon thermal transport in a graphene/MoSe<sub>2</sub> van der Waals heterobilayer, *Phys. Chem. Chem. Phys.*, 2018, **20**(4), 2637–2645.
- 84 J. A. Thomas, R. M. Iutzi and A. J. McGaughey, Thermal conductivity and phonon transport in empty and water-filled carbon nanotubes, *Phys. Rev. B: Condens. Matter Mater. Phys.*, 2010, **81**(4), 045413.
- 85 B. Mortazavi and T. Rabczuk, Multiscale modeling of heat conduction in graphene laminates, *Carbon*, 2015, **85**, 1–7.
- 86 Z. Fan, *et al.*, Thermal conductivity decomposition in two-dimensional materials: Application to graphene, *Phys. Rev. B*, 2017, **95**(14), 144309.
- 87 B. Mortazavi, *et al.*, Machine-learning interatomic potentials enable first-principles multiscale modeling of lattice thermal conductivity in graphene/borophene heterostructures, *Mater. Horiz.*, 2020, **7**(9), 2359–2367.
- 88 C. Si, *et al.*, Impacts of potential models on calculating the thermal conductivity of graphene using non-equilibrium molecular dynamics simulations, *Int. J. Heat Mass Transfer*, 2017, **107**, 450–460.
- 89 H. Zhang, G. Lee and K. Cho, Thermal transport in graphene and effects of vacancy defects, *Phys. Rev. B: Condens. Matter Mater. Phys.*, 2011, **84**(11), 115460.
- 90 G. Bouzerar, *et al.*, Drastic effects of vacancies on phonon lifetime and thermal conductivity in graphene, *J. Phys.: Condens. Matter*, 2020, **32**(29), 295702.
- 91 J.-W. Jiang, *et al.*, Isotopic effects on the thermal conductivity of graphene nanoribbons: Localization mechanism, *J. Appl. Phys.*, 2010, **107**(5), 054314.
- 92 J. Renteria, *et al.*, Anisotropy of Thermal Conductivity of Free-Standing Reduced Graphene Oxide Films Annealed at High Temperature, *arXiv*, 2015, preprint, arXiv:1503.07239, DOI: [10.48550/arXiv.1503.07239](https://doi.org/10.48550/arXiv.1503.07239).
- 93 W. Park, *et al.*, Electrical and thermal conductivities of reduced graphene oxide/polystyrene composites, *Appl. Phys. Lett.*, 2014, **104**(11), 113101.
- 94 F. Yousefi, F. Khoeini and A. Rajabpour, Thermal conductivity and thermal rectification of nanoporous graphene: A molecular dynamics simulation, *Int. J. Heat Mass Transfer*, 2020, **146**, 118884.
- 95 O. Farzadian, *et al.*, Thermal rectification in novel two-dimensional hybrid graphene/BCN sheets: A molecular dynamics simulation, *J. Mol. Graph. Model.*, 2024, **129**, 108763.
- 96 J. Hu, X. Ruan and Y. P. Chen, Thermal conductivity and thermal rectification in graphene nanoribbons: a molecular dynamics study, *Nano Lett.*, 2009, **9**(7), 2730–2735.
- 97 Y. Zhang, *et al.*, Interfacial thermal conductance and thermal rectification of hexagonal BC<sub>n</sub>N/graphene in-plane heterojunctions, *J. Phys. Chem. C*, 2018, **122**(39), 22783–22789.
- 98 S. Wu, *et al.*, Interfacial thermal conductance across graphene/MoS<sub>2</sub> van der Waals heterostructures, *Energies*, 2020, **13**(21), 5851.
- 99 S. Zeng, L.-Z. Zhang and J. Zhou, A coarse-grained simulation of heat and mass transfer through a graphene oxide-based composite membrane, *Chem. Eng. Sci.*, 2021, **243**, 116692.
- 100 R. Joshi, *et al.*, Precise and ultrafast molecular sieving through graphene oxide membranes, *Science*, 2014, **343**(6172), 752–754.
- 101 B. Mi, Graphene oxide membranes for ionic and molecular sieving, *Science*, 2014, **343**(6172), 740–742.
- 102 Q. Yang, *et al.*, Ultrathin graphene-based membrane with precise molecular sieving and ultrafast solvent permeation, *Nat. Mater.*, 2017, **16**(12), 1198–1202.
- 103 L.-Z. Zhang and Q.-W. Su, Performance manipulations of a composite membrane of low thermal conductivity for seawater desalination, *Chem. Eng. Sci.*, 2018, **192**, 61–73.
- 104 L.-Z. Zhang, S. Zeng and J. Zhou, A molecular level performance manipulation of thermal conductivity and moisture diffusivity through a composite membrane



- considering interfacial resistance, *J. Membr. Sci.*, 2019, **583**, 231–247.
- 105 C. D. Williams and M. Lísal, Coarse grained models of graphene and graphene oxide for use in aqueous solution, *2D Materials*, 2020, **7**(2), 025025.
- 106 G. Hummer, J. C. Rasaiah and J. P. Noworyta, Water conduction through the hydrophobic channel of a carbon nanotube, *Nature*, 2001, **414**(6860), 188–190.
- 107 A. Striolo, The mechanism of water diffusion in narrow carbon nanotubes, *Nano Lett.*, 2006, **6**(4), 633–639.
- 108 H. Tang, *et al.*, Effects of pH and electrolytes on the sheet-to-sheet aggregation mode of graphene oxide in aqueous solutions, *Environ. Sci.: Nano*, 2020, **7**(3), 984–995.
- 109 D. Wu and X. Yang, Coarse-grained molecular simulation of self-assembly for nonionic surfactants on graphene nanostructures, *J. Phys. Chem. B*, 2012, **116**(39), 12048–12056.
- 110 C.-J. Shih, *et al.*, Understanding the pH-dependent behavior of graphene oxide aqueous solutions: a comparative experimental and molecular dynamics simulation study, *Langmuir*, 2012, **28**(1), 235–241.
- 111 M. Poorsargol, *et al.*, Dispersion of graphene using surfactant mixtures: Experimental and molecular dynamics simulation studies, *Appl. Surf. Sci.*, 2019, **464**, 440–450.
- 112 M. Keshtkar, N. Mehdipour and H. Eslami, Supramolecular Self-Assembly of Dipalmitoylphosphatidylcholine and Carbon Nanotubes: A Dissipative Particle Dynamics Simulation Study, *Nanomaterials*, 2022, **12**(15), 2653.
- 113 C. D. Williams, F. R. Siperstein and P. Carbone, High-throughput molecular simulations reveal the origin of ion free energy barriers in graphene oxide membranes, *Nanoscale*, 2021, **13**(32), 13693–13702.
- 114 T. Dyer, N. Thamwattana and R. Jalili, Modelling the interaction of graphene oxide using an atomistic-continuum model, *RSC Adv.*, 2015, **5**(94), 77062–77070.
- 115 R. Devanathan, *et al.*, Molecular dynamics simulations reveal that water diffusion between graphene oxide layers is slow, *Sci. Rep.*, 2016, **6**(1), 29484.
- 116 F. Mouhat, F.-X. Coudert and M.-L. Bocquet, Structure and chemistry of graphene oxide in liquid water from first principles, *Nat. Commun.*, 2020, **11**(1), 1566.
- 117 B. Zhou, *et al.*, Simulation of dispersion and alignment of carbon nanotubes in polymer flow using dissipative particle dynamics, *Comput. Mater. Sci.*, 2017, **126**, 35–42.
- 118 R. Chawla and S. Sharma, Molecular dynamics simulation of carbon nanotube pull-out from polyethylene matrix, *Compos. Sci. Technol.*, 2017, **144**, 169–177.
- 119 A. Hente, *et al.*, A coarse-grained model for the elastic properties of cross linked short carbon nanotube/polymer composites, *Composites, Part B*, 2016, **95**, 404–411.
- 120 G. Gul, R. Faller and N. Ileri-Ercan, Coarse-grained modeling of polystyrene-modified CNTs and their interactions with lipid bilayers, *Biophys. J.*, 2023, **122**(10), 1748–1761.
- 121 F. Banhart, J. Kotakoski and A. V. Krasheninnikov, Structural defects in graphene, *ACS Nano*, 2011, **5**(1), 26–41.
- 122 V. H. Ho, D. T. Ho and S. Y. Kim, The effect of single vacancy defects on graphene nanoresonators, *Multiscale Sci. Eng.*, 2020, **2**(1), 1–6.
- 123 A. Juneja and G. Rajasekaran, Anomalous strength characteristics of Stone-Thrower-Wales defects in graphene sheets—a molecular dynamics study, *Phys. Chem. Chem. Phys.*, 2018, **20**(22), 15203–15215.
- 124 A. Verma and A. Parashar, The effect of STW defects on the mechanical properties and fracture toughness of pristine and hydrogenated graphene, *Phys. Chem. Chem. Phys.*, 2017, **19**(24), 16023–16037.
- 125 K. Mohammadi, *et al.*, Analysis of mechanical and thermal properties of carbon and silicon nanomaterials using a coarse-grained molecular dynamics method, *Int. J. Mech. Sci.*, 2020, **187**, 106112.
- 126 K. Gupta, *et al.*, Sparse machine learning assisted deep computational insights on the mechanical properties of graphene with intrinsic defects and doping, *J. Phys. Chem. Solids*, 2021, **155**, 110111.
- 127 A. E. Romanov, M. A. Rozhkov and A. L. Kolesnikova, Disclinations in polycrystalline graphene and pseudo-graphenes. Review, *Lett. Mater.*, 2018, **8**(4), 384–400.
- 128 N. Kumar, S. Verma, P. Kumar, A. A. Khan, J. Park and V. C. Srivastava, Efficient one-pot two-step electrochemical synthesis of highly oxidized graphene oxide for enhanced energy and environmental applications: Structure elucidation through DFT simulations, *Carbon*, 2024, **218**, 118722.
- 129 M. Pykal, *et al.*, Modelling of graphene functionalization, *Phys. Chem. Chem. Phys.*, 2016, **18**(9), 6351–6372.
- 130 B. Zheng, Z. Zheng and G. X. Gu, Scalable graphene defect prediction using transferable learning, *Nanomaterials*, 2021, **11**(9), 2341.
- 131 T. T. Tran, *et al.*, Mobility of single vacancies and adatoms in graphene at room temperature, *Small*, 2025, 2504370.
- 132 S. Su, *et al.*, Long-term evolution of vacancies in large-area graphene, *ACS Omega*, 2022, **7**(41), 36379–36386.
- 133 J.-J. Mao, *et al.*, Molecular dynamic simulation of defective graphene nanoribbons for tension and vibration, *Nanomaterials*, 2022, **12**(14), 2407.
- 134 X. Kong, *et al.*, The complementary graphene growth and etching revealed by large-scale kinetic Monte Carlo simulation, *npj Comput. Mater.*, 2021, **7**(1), 14.
- 135 B. N. Katz and V. Crespi, Healing of a topological scar: Coordination defects in a honeycomb lattice, *Carbon*, 2025, **238**, 120193.
- 136 E. Santos, Structural dynamics in the presence of water of graphene bilayers with defects, *Nanomaterials*, 2023, **13**(14), 2038.
- 137 D. Li, *et al.*, Fracture behavior of graphene with intrinsic defects and externally introduced defects, *Eng. Fract. Mech.*, 2024, **303**, 110130.
- 138 X. Liu, *et al.*, Investigation on fracture of pre-cracked single-layer graphene sheets, *Comput. Mater. Sci.*, 2019, **159**, 365–375.
- 139 J. Wang, *et al.*, Machine learning revealed giant thermal conductivity reduction by strong phonon localization in



- two-angle disordered twisted multilayer graphene, *npj Comput. Mater.*, 2025, **11**(1), 195.
- 140 Y. Guan and O. V. Yazyev, Electronic transport in graphene with out-of-plane disorder, *npj 2D Mater. Appl.*, 2024, **8**(1), 1.
- 141 M. R. Maamoon, *et al.*, A tight binding study of electron transport in notched graphene nanoribbons, *Sci. Rep.*, 2025, **15**(1), 19218.
- 142 Z. Fang, *et al.*, Nature of oxygen adsorption on defective carbonaceous materials, *J. Phys. Chem. C*, 2021, **125**(37), 20686–20696.
- 143 A. M. Kazakov, *et al.*, Molecular Dynamics Study on the Impact of Defects on Phonon Thermal Conductivity in Copper-Graphene Composites, *J. Micromech. Mol. Phys.*, 2025, **10**(01n02), 11–16.
- 144 B. Zheng and G. X. Gu, Machine learning-based detection of graphene defects with atomic precision, *Nano-Micro Lett.*, 2020, **12**(1), 181.
- 145 Z. Yang and M. J. Buehler, Linking atomic structural defects to mesoscale properties in crystalline solids using graph neural networks, *npj Comput. Mater.*, 2022, **8**(1), 198.
- 146 T. Xie and J. C. Grossman, Crystal graph convolutional neural networks for an accurate and interpretable prediction of material properties, *Phys. Rev. Lett.*, 2018, **120**(14), 145301.
- 147 C. Chen, *et al.*, Graph networks as a universal machine learning framework for molecules and crystals, *Chem. Mater.*, 2019, **31**(9), 3564–3572.
- 148 D. Jha, *et al.*, Elemnet: Deep learning the chemistry of materials from only elemental composition, *Sci. Rep.*, 2018, **8**(1), 17593.
- 149 Y. Zuo, *et al.*, Performance and cost assessment of machine learning interatomic potentials, *J. Phys. Chem. A*, 2020, **124**(4), 731–745.
- 150 D. Lu, *et al.*, 86 PFLOPS deep potential molecular dynamics simulation of 100 million atoms with ab initio accuracy, *Comput. Phys. Commun.*, 2021, **259**, 107624.
- 151 S. Batzner, *et al.*, E (3)-equivariant graph neural networks for data-efficient and accurate interatomic potentials, *Nat. Commun.*, 2022, **13**(1), 2453.
- 152 K. Schütt, *et al.*, SchNetPack: A deep learning toolbox for atomistic systems, *J. Chem. Theor. Comput.*, 2018, **15**(1), 448–455.
- 153 D. Plewczynski, S. A. Spieser and U. Koch, Performance of machine learning methods for ligand-based virtual screening, *Comb. Chem. High Throughput Screen.*, 2009, **12**(4), 358–368.
- 154 J. Wang and T. Hou, Recent advances on aqueous solubility prediction, *Comb. Chem. High Throughput Screen.*, 2011, **14**(5), 328–338.
- 155 A. Lusci, G. Pollastri and P. Baldi, Deep architectures and deep learning in chemoinformatics: the prediction of aqueous solubility for drug-like molecules, *J. Chem. Inf. Model.*, 2013, **53**(7), 1563–1575.
- 156 J. L. McDonagh, *et al.*, Uniting cheminformatics and chemical theory to predict the intrinsic aqueous solubility of crystalline druglike molecules, *J. Chem. Inf. Model.*, 2014, **54**(3), 844–856.
- 157 D. Eros, *et al.*, Reliability of logP predictions based on calculated molecular descriptors: a critical review, *Curr. Med. Chem.*, 2002, **9**(20), 1819–1829.
- 158 L. D. Hughes, *et al.*, Why are some properties more difficult to predict than others? A study of QSPR models of solubility, melting point, and Log P, *J. Chem. Inf. Model.*, 2008, **48**(1), 220–232.
- 159 R. Chen, *et al.*, Unified deep learning network for enhanced accuracy in predicting thermal conductivity of bilayer graphene, hexagonal boron nitride, and their heterostructures, *J. Appl. Phys.*, 2024, **135**(14), 145106.
- 160 W. Jin, *et al.*, Machine learning-based prediction of mechanical properties and performance of nickel-graphene nanocomposites using molecular dynamics simulation data, *ACS Appl. Nano Mater.*, 2023, **6**(13), 12190–12199.
- 161 S. Varma Siruvuri, *et al.*, Fracture strength of Graphene at high temperatures: data driven investigations supported by MD and analytical approaches, *Int. J. Mech. Mater. Des.*, 2022, **18**(4), 743–767.
- 162 P. Z. Hanakata, *et al.*, Accelerated search and design of stretchable graphene kirigami using machine learning, *Phys. Rev. Lett.*, 2018, **121**(25), 255304.
- 163 A. Khoei, M. Seddighian and A. R. Sameti, Machine learning-based multiscale framework for mechanical behavior of nano-crystalline structures, *Int. J. Mech. Sci.*, 2024, **265**, 108897.
- 164 S. Riniker, Molecular dynamics fingerprints (MDFP): machine learning from MD data to predict free-energy differences, *J. Chem. Inf. Model.*, 2017, **57**(4), 726–741.
- 165 O. T. Unke, *et al.*, Machine learning force fields, *Chem. Rev.*, 2021, **121**(16), 10142–10186.
- 166 H. Park, *et al.*, A generative artificial intelligence framework based on a molecular diffusion model for the design of metal-organic frameworks for carbon capture, *Commun. Chem.*, 2024, **7**(1), 21.
- 167 M. Deng, Z. Li, O. Borodin and G. E. Karniadakis, cDPD: a new dissipative particle dynamics method for modeling electrokinetic phenomena at the mesoscale, *J. Chem. Phys.*, 2016, **145**(14), 144109.
- 168 M. González-Melchor, *et al.*, Electrostatic interactions in dissipative particle dynamics using the Ewald sums, *J. Chem. Phys.*, 2006, **125**(22), 224107.
- 169 A. Gavrillov, A. Chertovich and E. Y. Kramarenko, Dissipative particle dynamics for systems with high density of charges: Implementation of electrostatic interactions, *J. Chem. Phys.*, 2016, **145**(17), 174101.
- 170 G. Faramarzi and N. Mehdipour, Metal–Nonmetal Transition in Fluid Cesium: A Many-Body Dissipative Particle Dynamics Simulation Approach, *J. Chem. Eng. Data*, 2017, **62**(11), 3938–3945.
- 171 A. C. Arias, *et al.*, Materials and applications for large area electronics: solution-based approaches, *Chem. Rev.*, 2010, **110**(1), 3–24.
- 172 J. Sun, B. Zhang and H. E. Katz, Materials for Printable, Transparent, and Low-Voltage Transistors, *Adv. Funct. Mater.*, 2011, **21**(1), 29–45.



- 173 M. Singh, *et al.*, Inkjet printing—process and its applications, *Adv. Mater.*, 2010, **22**(6), 673–685.
- 174 H. Yan, *et al.*, A high-mobility electron-transporting polymer for printed transistors, *Nature*, 2009, **457**(7230), 679–686.
- 175 J. W. Hennek, *et al.*, Reduced contact resistance in inkjet printed high-performance amorphous indium gallium zinc oxide transistors, *ACS Appl. Mater. Interfaces*, 2012, **4**(3), 1614–1619.
- 176 C. N. Hoth, *et al.*, High photovoltaic performance of inkjet printed polymer: fullerene blends, *Adv. Mater.*, 2007, **19**(22), 3973–3978.
- 177 C. N. Hoth, *et al.*, Printing highly efficient organic solar cells, *Nano Lett.*, 2008, **8**(9), 2806–2813.
- 178 V. Wood, *et al.*, Quantum Dot–Polymer Composites for Displays: Inkjet-Printed Quantum Dot–Polymer Composites for Full-Color AC-Driven Displays (*Adv. Mater.* 21/2009), *Adv. Mater.*, 2009, **21**(21), 2151.
- 179 L. L. Lavery, G. L. Whiting and A. C. Arias, All ink-jet printed polyfluorene photosensor for high illuminance detection, *Org. Electron.*, 2011, **12**(4), 682–685.
- 180 V. Dua, *et al.*, All-organic vapor sensor using inkjet-printed reduced graphene oxide, *Angew. Chem.*, 2010, **122**(12), 2200–2203.
- 181 K. S. Novoselov, *et al.*, A roadmap for graphene, *Nature*, 2012, **490**(7419), 192–200.
- 182 I. N. Kholmanov, *et al.*, Improved electrical conductivity of graphene films integrated with metal nanowires, *Nano Lett.*, 2012, **12**(11), 5679–5683.
- 183 C. a. Di, *et al.*, Patterned graphene as source/drain electrodes for bottom-contact organic field-effect transistors, *Adv. Mater.*, 2008, **20**(17), 3289–3293.
- 184 F. Torrisi, *et al.*, Inkjet-printed graphene electronics, *ACS Nano*, 2012, **6**(4), 2992–3006.
- 185 S.-K. Lee, *et al.*, Stretchable graphene transistors with printed dielectrics and gate electrodes, *Nano Lett.*, 2011, **11**(11), 4642–4646.
- 186 B. J. Kim, *et al.*, Coplanar-gate transparent graphene transistors and inverters on plastic, *ACS Nano*, 2012, **6**(10), 8646–8651.
- 187 X. Li, *et al.*, Highly conducting graphene sheets and Langmuir–Blodgett films, *Nat. Nanotechnol.*, 2008, **3**(9), 538–542.
- 188 Y. Hernandez, *et al.*, High-yield production of graphene by liquid-phase exfoliation of graphite, *Nat. Nanotechnol.*, 2008, **3**(9), 563–568.
- 189 G. Eda, G. Fanchini and M. Chhowalla, Large-area ultrathin films of reduced graphene oxide as a transparent and flexible electronic material, *Nat. Nanotechnol.*, 2008, **3**(5), 270–274.
- 190 D. Li, *et al.*, Processable aqueous dispersions of graphene nanosheets, *Nat. Nanotechnol.*, 2008, **3**(2), 101–105.
- 191 X. Wang, L. Zhi and K. Müllen, Transparent, conductive graphene electrodes for dye-sensitized solar cells, *Nano Lett.*, 2008, **8**(1), 323–327.
- 192 S. Stankovich, *et al.*, Graphene-based composite materials, *Nature*, 2006, **442**(7100), 282–286.
- 193 S. Lim, *et al.*, Inkjet-printed reduced graphene oxide/poly (vinyl alcohol) composite electrodes for flexible transparent organic field-effect transistors, *J. Phys. Chem. C*, 2012, **116**(13), 7520–7525.
- 194 D. Kong, *et al.*, Temperature-dependent electrical properties of graphene inkjet-printed on flexible materials, *Langmuir*, 2012, **28**(37), 13467–13472.
- 195 K. Y. Shin, J. Y. Hong and J. Jang, Micropatterning of graphene sheets by inkjet printing and its wideband dipole-antenna application, *Adv. Mater.*, 2011, **23**(18), 2113–2118.
- 196 C. Gómez-Navarro, *et al.*, Electronic transport properties of individual chemically reduced graphene oxide sheets, *Nano Lett.*, 2007, **7**(11), 3499–3503.
- 197 C. Mattevi, *et al.*, Evolution of electrical, chemical, and structural properties of transparent and conducting chemically derived graphene thin films, *Adv. Funct. Mater.*, 2009, **19**(16), 2577–2583.
- 198 Y. Hernandez, *et al.*, Measurement of multicomponent solubility parameters for graphene facilitates solvent discovery, *Langmuir*, 2010, **26**(5), 3208–3213.
- 199 N. Behabtu, *et al.*, Spontaneous high-concentration dispersions and liquid crystals of graphene, *Nat. Nanotechnol.*, 2010, **5**(6), 406–411.
- 200 A. A. Green and M. C. Hersam, Solution phase production of graphene with controlled thickness via density differentiation, *Nano Lett.*, 2009, **9**(12), 4031–4036.
- 201 Y. T. Liang and M. C. Hersam, Highly concentrated graphene solutions via polymer enhanced solvent exfoliation and iterative solvent exchange, *J. Am. Chem. Soc.*, 2010, **132**(50), 17661–17663.
- 202 J.-W. T. Seo, *et al.*, High-concentration aqueous dispersions of graphene using nonionic, biocompatible block copolymers, *J. Phys. Chem. Lett.*, 2011, **2**(9), 1004–1008.
- 203 M. Lotya, *et al.*, Liquid phase production of graphene by exfoliation of graphite in surfactant/water solutions, *J. Am. Chem. Soc.*, 2009, **131**(10), 3611–3620.
- 204 E. B. Secor, *et al.*, Inkjet printing of high conductivity, flexible graphene patterns, *J. Phys. Chem. Lett.*, 2013, **4**(8), 1347–1351.
- 205 J. Li, *et al.*, Efficient inkjet printing of graphene, *Adv. Mater.*, 2013, **25**(29), 3985–3992.
- 206 Y. Gao, *et al.*, Inkjet printing patterns of highly conductive pristine graphene on flexible substrates, *Ind. Eng. Chem. Res.*, 2014, **53**(43), 16777–16784.
- 207 E. B. Secor, *et al.*, Rapid and versatile photonic annealing of graphene inks for flexible printed electronics, *Adv. Mater.*, 2015, **27**(42), 6683–6688.
- 208 E. B. Secor, *et al.*, Enhanced conductivity, adhesion, and environmental stability of printed graphene inks with nitrocellulose, *Chem. Mater.*, 2017, **29**(5), 2332–2340.
- 209 L. Wu, *et al.*, A Molecular Dynamics Simulation Study: The Inkjet Printing of Graphene Inks on Polyimide Substrates, *Front. Mater.*, 2021, **8**, 769071.



## Review

- 210 Z. Chen, *et al.*, Physics-informed machine learning enabled virtual experimentation for 3D printed thermoplastic, *Mater. Horiz.*, 2024, **11**(23), 6028–6039.
- 211 D. Frenkel and B. Smit, *Understanding Molecular Simulation: from Algorithms to Applications*, Elsevier, 2023.
- 212 G. A. Voth, *Coarse-graining of Condensed Phase and Biomolecular Systems*, CRC press, 2008.
- 213 J. Wei, *et al.*, Machine learning in materials science, *InfoMat*, 2019, **1**(3), 338–358.
- 214 H. Ye, W. Xian and Y. Li, Machine learning of coarse-grained models for organic molecules and polymers: Progress, opportunities, and challenges, *ACS Omega*, 2021, **6**(3), 1758–1772.
- 215 Y. Wang, K. Niu and Y. Wu, Multiscale modelling of graphene sheet and its application in laminated composites, *Compos. Struct.*, 2021, **276**, 114416.
- 216 M. Majewski, *et al.*, Machine learning coarse-grained potentials of protein thermodynamics, *Nat. Commun.*, 2023, **14**(1), 5739.
- 217 A. B. Poma, *et al.*, Recent Advances in Machine Learning and Coarse-Grained Potentials for Biomolecular Simulations and Their Applications, *Biophys. J.*, 2025, **125**, 327–343.
- 218 Y. Ge, *et al.*, Coarse-grained models for ionic liquids and applications to biological and electrochemical systems, *Ind. Chem. Mater.*, 2025, 383–413.
- 219 D. G. Papageorgiou, I. A. Kinloch and R. J. Young, Mechanical properties of graphene and graphene-based nanocomposites, *Prog. Mater. Sci.*, 2017, **90**, 75–127.
- 220 F. Bonaccorso, *et al.*, Graphene photonics and optoelectronics, *Nat. Photonics*, 2010, **4**(9), 611–622.
- 221 M. D. Stoller, *et al.*, Graphene-based ultracapacitors, *Nano Lett.*, 2008, **8**(10), 3498–3502.
- 222 E. Yoo, *et al.*, Large reversible Li storage of graphene nanosheet families for use in rechargeable lithium ion batteries, *Nano Lett.*, 2008, **8**(8), 2277–2282.
- 223 N. Wei, *et al.*, Strain engineering of thermal conductivity in graphene sheets and nanoribbons: ademonstration of magic flexibility, *Nanotechnology*, 2011, **22**(10), 105705.
- 224 M. Chhowalla, D. Jena and H. Zhang, Two-dimensional semiconductors for transistors, *Nat. Rev. Mater.*, 2016, **1**(11), 1–15.

